Research Square

Preprints are preliminary reports that have not undergone peer review.
They should not be considered conclusive, used to inform clinical practice,
or referenced by the media as validated information.

Green Synthesis of Zinc Oxide Nanoparticles and Evaluation of Their Antifungal Activity and Seed Nanopriming Effects

Jyoti Singh
Chaudhary Charan Singh University
Ankit Kumar
Chaudhary Charan Singh University
Akash Gaurav
Chaudhary Charan Singh University
Dharmendra Pratap
virologyccsu@gmail.com

Chaudhary Charan Singh University

Research Article

Keywords:

Posted Date: May 19th, 2026

DOI: https://doi.org/10.21203/rs.3.rs-9576637/v1

License: This work is licensed under a Creative Commons Attribution 4.0 International License.
Read Full License

Additional Declarations: No competing interests reported.

Green Synthesis of Zinc Oxide Nanoparticles and Evaluation of Their Antifungal Activity and Seed Nanopriming Effects

[1]Jyoti Singh, [1,2]Ankit Kumar, [1]Akash Gaurav, [1*]Dharmendra Pratap

[1]Department of Genetics and Plant Breeding, Chaudhary Charan Singh University, Meerut, Uttar Pradesh 250004, India
[2]International Center for Genetic Engineering and Biotechnology, Aruna Asaf Ali Marg, New Delhi 110067, India

Corresponding email: virologyccsu@gmail.com

Abstract

Background Fungal phytopathogens pose serious threat to agricultural productivity worldwide, and the use of conventional fungicides is declining due to the emergence of resistant pathogens and environmental hazards. Green synthesized nanoparticles have emerged as promising alternatives owing to their unique nanoscale characteristics, particularly their high surface reactivity and capacity to generate reactive oxygen species (ROS), which contribute to their antifungal activity. zinc oxide nanoparticles (ZnONPs) also serve as a source of zinc, an essential micronutrient involved in numerous physiological and enzymatic processes in plants. The present study investigates the green synthesis of ZnONPs using *Azadirachta indica* and evaluates their role in fungal inhibition and plant growth enhancement.

Results The synthesized ZnONPs displayed a characteristic absorption peak at 390 nm, predominantly spherical morphology, a particle size range of 12.28–17.5 nm, and high elemental purity (83.07% Zn, 16.93% O). ZnONPs exhibited strong antifungal activity under *in vitro* conditions, achieving up to 100% inhibition against *Rhizoctonia solani*, *Sclerotinia sclerotiorum*, *Colletotrichum falcatum*, and upto 80% inhibition against *C. gloeosporioides*. In detached assays, ZnONPs significantly reduced disease severity, with 73.95–81.16% inhibition of anthracnose in *Mangifera indica* and up to 100% suppression of *R. solani* in *Zea mays* and *Oryza sativa*. Nanopriming with synthesized ZnONPs also enhanced germination and different morphological traits in *Triticum aestivum*, *Cicer arietinum*, *Solanum lycopersicum*, and *Brassica nigra*. However, higher concentrations induced species-specific phytotoxic effects, indicating the necessity of dosage optimization.

Conclusions Green synthesized ZnONPs offer broad-spectrum antifungal activity and support plant growth through nanopriming. However, the concentration- and species-dependent phytotoxic effects observed highlight the importance of optimizing application rates, along with the need for further studies and validation under field conditions before large-scale use.

Background

Fungal diseases pose a serious challenge to agricultural sustainability, significantly reducing crop yields and contributing to major losses in global food production [1, 2]. In India, soil- and seed-borne fungi are responsible for significant yield reductions, posing a serious challenge to sustainable agriculture [3]. *Rhizoctonia solani* is a soil- and seed-borne necrotrophic fungal pathogen causing banded leaf and sheath blight (BLSB) of maize and sheath blight of rice [4]. Its wide host range, persistent survival in soil and plant debris, and ability to colonize alternate hosts significantly complicate effective disease

management [5]. *Sclerotinia sclerotiorum* is a soil-borne necrotrophic pathogen with a broad host range of crops [6, 7]. *Colletotrichum falcatum* is a soil-borne pathogen responsible for red rot of sugarcane in tropical and subtropical regions, causing significant yield and quality losses, particularly in the Indian subcontinent [8, 9]. *C. gloeosporioides*, a seed-borne hemibiotrophic pathogen, is the causal agent of anthracnose in a wide range of crops, leading to significant pre- and post-harvest losses [10]. These pathogens cause substantial yield and quality losses in a wide range of economically important crops, often resulting in severe economic losses (30–50%) and, under favourable environmental conditions, leading to partial or complete crop failure [11, 12].

Plant fungal diseases are managed using chemical fungicides, biological control agents, and resistant cultivars [13]. However, excessive fungicide use has resulted in environmental contamination and the emergence of resistant pathogen populations, limiting their long-term usage [14]. Although biocontrol agents and post-harvest treatments such as cold storage, plant extracts, and modified atmospheres show promise, their effectiveness remains limited [15, 16].

These challenges highlight the need for sustainable and effective antifungal alternatives with reduced environmental risk [17]. Nanotechnology has emerged as a promising tool for plant disease management and crop improvement, offering opportunities for reduced chemical inputs and improved delivery efficiency [18]. Nanoparticles can reduce dependence on conventional agrochemicals while providing effective control of phytopathogens and enhancing plant growth and nutrient efficiency [19]. Nanofungicides, particularly biogenic formulations, provide advantages such as targeted delivery, low-dose application, and controlled release, improving efficacy while minimizing non-target effects [20, 21]. Nonetheless, potential food-chain transfer of nanomaterials necessitates thorough safety evaluation prior to large-scale agricultural use [22, 23].

Nanoparticles (1–100 nm range), exhibiting physicochemical properties distinct from their bulk counterparts [24]. Metal oxide nanoparticles, particularly zinc oxide nanoparticles (ZnONPs), have gained attention due to their biocompatibility, cost-effectiveness, and broad applications in agriculture [25]. ZnONPs possess a wide band gap (3.37 eV), high exciton binding energy (60 meV), high surface-area-to-volume ratio, and strong antimicrobial activity, largely attributed to reactive oxygen species generation [26]. Zinc is an essential micronutrient for plants and a trace element in human physiology, and the biocompatibility of ZnONPs arises from the low toxicity and biodegradability of soluble Zn^{2+} ions [27]. Zinc is an essential micronutrient, and ZnO-based formulations are generally regarded as having low toxicity; however, the safety of ZnONPs in agricultural applications depends strongly on particle size, dose, and exposure route [28].

Green synthesis of ZnONPs offers an eco-sustainable alternative to conventional physico-chemical methods by using biological reducing and stabilizing agents, thereby minimizing environmental and health risks [29]. Plant extracts are particularly suitable due to their rich phytochemical content, cost-effectiveness, simplicity, and ability to control nanoparticle size and morphology [30]. Compared with microbial routes, plant-based synthesis is safer and more practical for large-scale production [31].

Azadirachta indica (*Meliaceae*), commonly known as neem, is widely distributed in India and is rich in bioactive phytochemicals with antimicrobial properties. *A. indica* leaf extract acts as a reducing, capping, and stabilizing agent, with terpenoids and flavonoids facilitating nanoparticle synthesis and stabilization [32]. *A. indica* is extensively explored for the green synthesis of ZnONPs [33, 34] and previous studies have provided valuable insights to the synthesis of ZnONPs using *A. indica* extract primarily using low precursor concentration [35–37] and did not evaluate the nanoparticle purity, dispersibility and their bioefficacy for agricultural applications [38–40].

Nanoparticles can also enhance nutrient use efficiency due to their small size, high surface area, and controlled release properties [41]. However, their effects on plants are highly dependent on particle type, size, concentration, and plant species [42]. Among delivery strategies, seed priming with nanoparticles, i.e., nanopriming, has emerged as an effective method to improve germination, seedling

vigor, and stress tolerance [43]. Conventional seed priming techniques, including hydropriming, hormonal priming, nutrient priming, and osmopriming, are widely used but show variable efficiency across crops [44]. ZnONPs have been explored for their potential to modulate plant growth and micronutrient availability; however, their biological effects are highly concentration and species-dependent [45]. Previous, studies reported that the effects of nanoparticles on plants can be both positive and negative, depending on factors such as chemical composition, size, reactivity, dose, and plant species [46]. Nevertheless, ZnONPs due to their high reactivity and solubility, serve as a promising alternative to conventional zinc fertilizers, addressing zinc deficiencies in plants and improving crop yields [47]. Zinc is an essential micronutrient involved in enzymatic activity, photosynthesis, antioxidant defense, and growth regulation, and ZnONPs improve zinc uptake due to their higher reactivity and solubility [48]. At optimal concentrations, ZnONPs enhance germination, growth, and photosynthetic performance, whereas higher doses may induce phytotoxic effects, emphasizing the need for precise dose optimization [49].

Nanopriming demonstrates significant promise for sustainable agriculture [50]. Seeds of *Triticum aestivum* (wheat), *Cicer arietinum* (chickpea), *Solanum lycopersicum* (tomato), and *Brassica nigra* (black mustard) were selected to represent major crop groups with distinct seed structures, germination physiology and contrasting susceptibility to fungal diseases. These crops also differ in their vulnerability to soil- and seed-borne pathogens, including species evaluated in the present study. The biological responses to ZnONPs are highly dependent on particle size, concentration, and plant species [51]. However, studies about its long-term phytotoxic effects are limited. Further research is therefore required to evaluate the safety, effectiveness, and potential phytotoxicity of ZnONPs, particularly their bioaccumulation effects in plants to ensure their safe and effective integration into crop production systems [52, 53].

Although *A. indica* mediated synthesis of ZnONPs has been reported previously, most studies did not evaluate nanoparticle purity, dispersibility, long-term stability, and their agricultural bioefficacy [37, 54]. Notably, prior studies have not combined *in vitro* antifungal assays, detached tissue assays, and seed nanopriming within a single experimental framework. To address these gaps, the present study synthesizes ZnONPs from a high molarity precursor, evaluates their purity and dispersibility, and examines their antifungal activity against four major phytopathogens using both *in vitro* assays and detached fruit and leaf bioassays. The potential nanofertilizer effect of the ZnONPs is assessed through seed nanopriming in four crop species, focusing on early growth parameters. The present study links green synthesis of ZnONPs with agricultural applications and demonstrated their antifungal and plant growth promoting potential, while also highlighting the need for future *in vivo* and field-scale validation.

Materials and Methods

Chemicals

Zinc nitrate hexahydrate [$Zn(NO_3)_2 \cdot 6H_2O$] was procured from Merk, India. Trisodium citrate, ethanol, sodium hydroxide (NaOH), potato dextrose agar (PDA), carbendazim, mancozeb, and kanamycin were purchased from Himedia Laboratories, India. Seeds of *T. aestivum*, *C. arietinum*, and *B. nigra* were procured from the Department of Genetics and Plant Breeding, Chaudhary Charan Singh University, Meerut, Uttar Pradesh, India. The seeds of *S. lycopersicum* were procured from the local market of Meerut, Uttar Pradesh, India. Whatman No. 1 filter paper was procured from Sigma Aldrich, USA.

Collection of *A. indica* leaves and preparation of aqueous leaf extract

Healthy and fresh leaves of *A. indica* were collected from the research fields of Chaudhary Charan Singh University, Meerut, Uttar Pradesh. The collected leaves were thoroughly washed 3 to 5 times with tap water, followed of double-distilled water, to eliminate impurities such as debris, dirt, and

particulate matter from the leaf surface. Leaves were shade-dried at room temperature for 5–8 days and ground into powder. Aqueous leaf extract was prepared by cold maceration, mixing 25 g of leaf powder with 500 ml double-distilled water, followed by 24 h incubation at 25 °C with agitation at 250–350 rpm. The crude extract obtained was filtered three times using Whatman No. 1 filter paper to remove particulate matter and obtained an aqueous solution of plant leaf extract. The leaf extract was stored at 4 °C and used for the green synthesis of ZnONPs.

Green synthesis of ZnONPs

The aqueous leaf extract of *A. indica* (25 mL) was heated to 55 °C under constant stirring, after which 5 g of $Zn(NO_3)_2 \cdot 6H_2O$ was added to the extract. After 3 h of continuous stirring, 0.1 g NaOH was added to the reaction mixture. The obtained precipitate was aged for 24 h, then centrifuged at 6500 rpm for 15 min. The obtained pellet was washed 3 to 4 times with double distilled water and dried overnight at 45°C. The obtained powdered form of ZnONPs was used for further characterization. Powdered ZnONPs were dispersed in 5% trisodium citrate and evaluated for the antifungal and nanopriming activity. The ZnONPs were also calcinated at 400 °C for 2 h in a muffle furnace and stored at room temperature for XRD characterization.

Characterization of ZnONPs

UV-Visible Spectroscopy

The optical properties of ZnONPs synthesized via the bio-reduction of zinc (Zn^{2+}) ions using aqueous leaf extract of *A. indica* were evaluated using a UV-Vis spectrophotometer (Lasany International, F825R12HB). For absorbance measurements, small aliquots from the ZnONPs and leaf extract were transferred into a quartz cuvette (1 cm path length) and measured at room temperature. UV-Vis spectral analysis was carried out within the 200–800 nm range at a spectral resolution of 1 nm [55].

Fourier Transform Infrared Spectroscopy

FTIR analysis was carried out using a PerkinElmer FTIR L1600300 (Llantrisant, U.K.) spectrophotometer in the wavenumber range of 4000–400 cm^{-1}, utilizing the attenuated total reflectance (ATR) mode. The FTIR spectrum of *A. indica* leaf extract was compared with ZnONPs to elucidate the functional moieties involved in the surface capping and stabilization of the synthesized ZnONPs.

Field Emission Scanning Electron Microscopy and Energy Dispersive X-ray Spectroscopy

The surface morphology of the synthesized ZnONPs was determined using FESEM (Carl Zeiss, Ultra Plus series). For FESEM analysis of ZnONPs, a beam energy of 10 kV was applied. The samples were analyzed at working distances of 1 µm and 200 nm, with magnifications of 25,000× and 1,00,000×, respectively. EDX spectroscopy was used to analyzed the elemental composition of the synthesized ZnONPs.

X-ray Diffraction

XRD revealed the arrangement of atoms inside the crystallographic structure of the ZnONPs by measuring their X-ray diffraction patterns. The structure, phases, size, and crystallinity of the calcinated ZnONPs were analyzed using XRD (Bruker AXS, D8 Advance). The XRD pattern was recorded using graphite monochromatized high-density Cu Kα radiation (λ = 1.5406 Å) across a 2θ range of 20° to 80°. The average crystallite size of the synthesized ZnONPs was calculated from the full-width half maximum and Bragg reflections by using the following Debye-Scherrer equation [56]:

$$D = K\lambda/\beta\cos\theta$$

where, D denotes the crystal size estimated from the XRD patterns, θ represents the Bragg angle in degrees, λ denotes the wavelength of the X-ray source used (1.5406 Å), and β refers to the full width at half maximum (FWHM) of the diffraction peak, measured in radians, and constant K (geometric factor) is equal to 0.9424.

Transmission Electron Microscopy

The morphology and particle size of the synthesized ZnONPs were analyzed using TEM (JEOL JEM-1400) operating at 120 kV. Carbon-coated copper grids were used for sample preparation. For the sample preparation, a drop of ZnONPs was placed on the grids and dried at ambient temperature. After the sample dried and formed a partially transparent layer, the sample was examined, and images were obtained from the shadow of the electron beam interacting with the sample [57]. Particle size analysis was conducted using ImageJ to calculate the average dimensions.

***In vitro* antifungal assay**

Pure fungal cultures of *R. solani* (ITCC No. 7855), *S. sclerotiorum* (ITCC No. 447), *C. falcatum* (ITCC No. 4800), and *C. gloeosporioides* (ITCC No. 6933) were procured. The antifungal activity of ZnONPs (10–2000 mg L^{-1}) was evaluated *in vitro* using the poisoned food technique on PDA media. The hyphae of the actively growing mycelium of a 5 to 8-day-old fungal culture were inoculated at the center of the petri dish. Trisodium citrate (5000 mg L^{-1}) served as a negative control, while carbendazim and mancozeb (200 mg L^{-1}) were used as positive control. All control and treatment media contained equivalent volumes of trisodium citrate. Plates were incubated for 7 days at 28 ± 2 °C for the antifungal analysis against *R. solani*, *C. falcatum*, and *C. gloeosporioides,* and at 25 ± 2 °C for the antifungal analysis against *S. sclerotiorum*. The circular growth of mycelium was measured after 3, 5, and 7 days of incubation. All treatments were performed in triplicate [58]. The percent inhibition of fungi was determined using the following formula [59]:

$$\text{Growth inhibition (\%)} = \frac{\mathrm{C} - \mathrm{T}}{\mathrm{C}} \times 100$$

where, C represents the average mycelial growth in control petri plates, and T represents the average mycelial growth in treated petri plates.

Detached fruit assay against *C. gloeosporioides* on *Mangifera indica*

Semi-ripe, disease-free mango fruits of uniform size were collected from a mango tree taxonomically identified and maintained by the Department of Botany, Chaudhary Charan Singh University, Meerut. Following thorough washing in running water, fruits were surface sterilized with 0.1% sodium hypochlorite (2 min) and 70% ethanol (2 min), then rinsed three times with sterile distilled water and air-dried. Each fruit was wounded at both ends (2 mm depth) using a sterile needle, then treated by immersing in ZnONPs (500–2000 mg L^{-1}) for 10 min. After air drying, wounds were inoculated with 20 µL of *C. gloeosporioides* spore suspension (1 × 10^6 spores/mL). Controls included wounded/inoculated (control) and unwounded/uninoculated (untreated) fruits. All fruits were maintained at 24 ± 1°C with ~95% relative humidity (RH) for 7 days using sterile distilled water in plastic containers (45 cm × 40 cm × 15 cm) [60]. Lesion development was assessed by measuring lesion size (mm) at each infection site, with the experiment conducted in triplicate (8 fruits per replicate, 24 fruits total per treatment) following established protocols with some modifications. After 7 days of post-inoculation, the percentage of inhibition of the fungal growth on the treated and control mango fruits was calculated using the following formula:

$$\text{Percentage of Inhibition} = \frac{\text{DC} - \text{T}}{\text{DC}} \times 100$$

where, DC represents the lesion size on diseased control fruit, and T represents the lesion size on treated fruit.

The grades or scores ranged from 0 to 5, representing the affected or diseased fruit areas (DFA) of 0%, ≤20%, 21–40%, 41–60%, 61–80%, and >80%, respectively [16].

Detached leaf assay against *R. solani* on *Zea mays* and *Oryza sativa*

Healthy leaves from 45-day-old maize and rice plants were collected from the research fields of the Department of Genetics and Plant Breeding, Meerut, India. Leaves were cut into 6 cm segments, surface-sterilized sequentially with 0.5% sodium hypochlorite (2 min) and 70% ethanol (2 min), then rinsed thrice with sterile distilled water and air-dried. Both leaf surfaces were uniformly coated with ZnONPs (500–2000 mg L^{-1}; 1 mL/leaf) using a sterile paintbrush, with sterile distilled water as a control. Segments were placed abaxial-side up on 0.7% water agar in petri dishes and pre-incubated at 25 ±2°C for 24 h. After incubation, treated and control leaves were inoculated with *R. solani* spores (1×10^6 spores/mL; 500 µL/leaf). Untreated leaves remained uninoculated. Sealed plates were maintained at 25 ±2°C with 90% RH under 16/8 h light/dark cycles [61]. Each treatment consisted of three biological replicates. After 4 days of post-inoculation, the percentage of disease incidence of the fungal growth on the treated and control leaf and the percentage of disease reduction were calculated using the following formulas [62]:

$$\text{Percent disease incidence (PDI)} = \frac{\text{Lesion length}}{\text{Leaf segment length}} \times 100$$

$$\text{Percent disease reduction (PDR)} = \frac{\text{PDI in diseased control} - \text{PDI in nanoformulations treated}}{\text{PDI in diseased control}} \times 100$$

Based on the diseased leaf area (DLA), the grade or score of BLSB or sheath blight incidence was calculated using a 0–9 rating scale provided by the International Rice Research Institute [63] where 0 = no infection, 1 = lesions limited ≤20%, 3 = 20–30%, 5 = 31–45%, 7 = 46–65%, and 9 = >65% infected leaf area.

Nanopriming of seeds with ZnONPs

Seeds of *T. aestivum*, *C. arietinum*, *S. lycopersicum*, and *B. nigra* were used to evaluate the effects of nanopriming. Three treatments were used: untreated seeds (unprimed, control), water treated seeds (hydroprimed), and ZnONPs treated seeds (nanoprimed) [43]. For surface sterilization, seeds of *T. aestivum* and *C. arietinum* were treated with 2% sodium hypochlorite for 2 min, whereas seeds of *S. lycopersicum* and *B. nigra* were treated for 30 s. All seeds were rinsed 5–7 times with deionized water to eliminate residual chlorine. For seed nanopriming, seeds were soaked in ZnONPs suspensions (100 and 500 mg L^{-1}) at 25 °C for 18 h in the dark under gentle agitation. Hydropriming was performed with deionized water. Following priming, seeds were rinsed 3–4 times with distilled water (3 min each wash) and dried back to their original moisture content.

Three seeds per pot (3 seeds per replicate, 9 seeds per treatment) were sown in autoclaved sand. All pots were maintained under greenhouse conditions (23 ± 2 °C, 16:8 h light/dark photoperiod, 85–90% RH) for 21 days. Tap water was used for irrigation across all treatments. Germination percentage was recorded after 7 days, while morphological traits were assessed after 21 days.

Effect of Nanoprimed ZnONPs on Germination

Seed germination was recorded, and the number of germinated seeds was counted until no further germination was observed (7 days). The germination percentage was calculated using the following formula [64]:

$$\text{Germination (\%)} = \frac{\text{Number of seeds germinated}}{\text{Total number of seeds}} \times 100$$

Effect of Nanoprimed ZnONPs on Root and Shoot Length

Root and shoot lengths were measured 21 days after seed transfer to pots. Plants were carefully uprooted to avoid damage, and data was recorded using a millimetre scale. Root length was measured from the point of emergence to the root tip, while shoot length was measured from the base to the apex.

Effect of Nanoprimed ZnONPs on Root and Shoot Biomass

Fresh root and shoot samples were harvested 21 days after seed transfer, separated, thoroughly cleaned, and weighed to determine fresh biomass (mg plant^{-1}). Samples were then oven dried at 40 °C for 72 h to constant weight, and dry biomass was recorded (mg plant^{-1}).

Statistical analysis

All data were analyzed using SPSS (v25), RStudio (v4.3.1), and Python (v3.10.12). For *in vitro* antifungal studies, a three-way ANOVA (univariate general linear model) was employed. MANOVA (multivariate general linear model) was also applied for simultaneous evaluation of correlated disease parameters (lesion size, incidence, etc.). A one-way ANOVA was utilized to evaluate the ZnONPs effect on germination and morphological traits in the greenhouse trial across four different crops. Post-hoc comparisons were performed with Tukey's test at the significant threshold ($p < 0.05$). The completely randomized design (CRD) was implemented for all experiments, with ≥3 replicates per treatment. Results are presented as mean ± standard error. Dose-response relationship (half maximal effective concentration, EC_{50} values) was estimated through nonlinear regression using the four-parameter logistic (4PL) model fitted to normalized response curves in GraphPad Prism (v10), with data visualization in OriginPro (v9.0).

Results

Green Synthesis of ZnONPs

The synthesis of ZnONPs was initially indicated by distinct visual changes from reddish-brown plant leaf extract to the yellow color of ZnONPs suspension. ZnONPs were synthesized in powdered form, with yields of approximately 55–65%. The green synthesized ZnONPs exhibited complete dispersity in 5% aqueous solutions of trisodium citrate. Notably, no sedimentation or phase separation was observed, indicating a uniform and stable nanoparticle dispersion (Fig. 1).

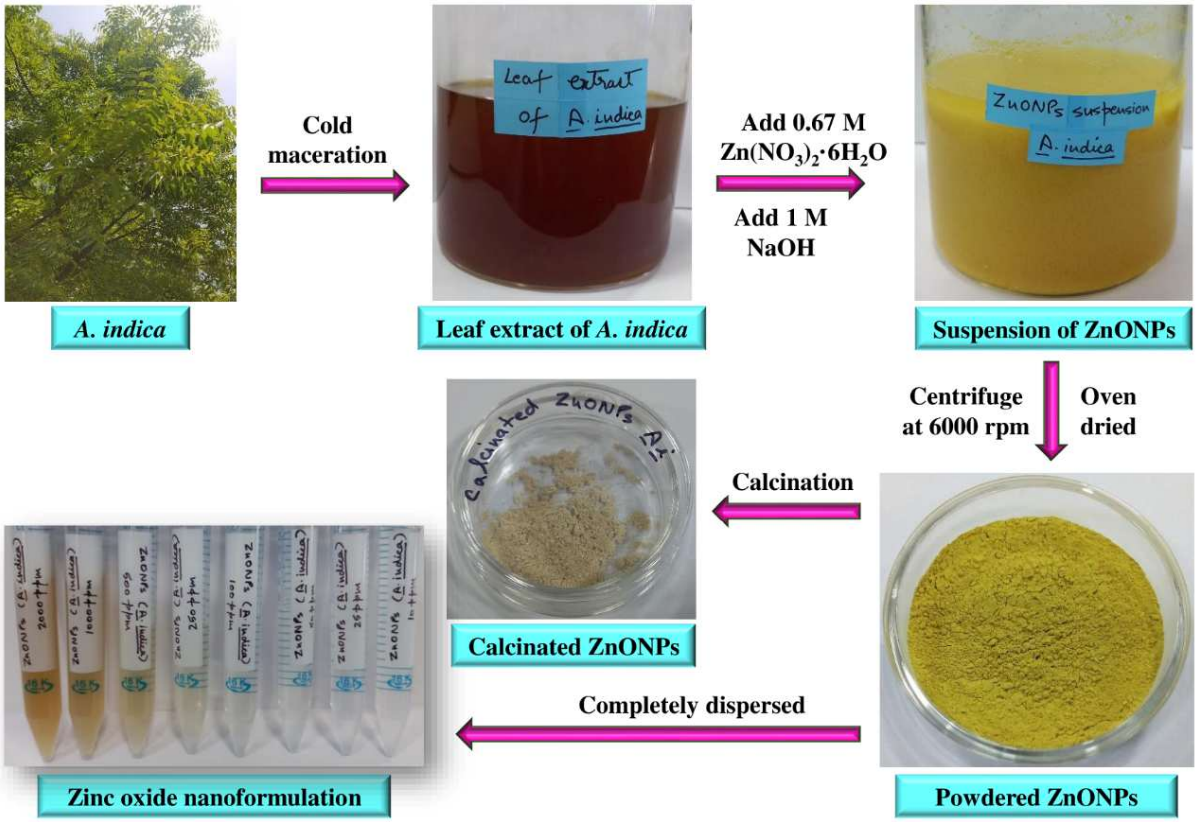


Fig. 1. Schematic representation of green synthesis of ZnONPs using *Azadirachta indica* leaf extract.

Characterization of ZnONPs

UV-Vis Spectroscopy analysis of ZnONPs

The UV-Vis spectrum of ZnONPs showed distinct absorption peak at 390 nm, indicating the successful synthesis of ZnONPs. The UV-Vis spectrum of *A. indica* leaf extract showed absorption peaks at 240 nm, 290 nm, and 420 nm, indicative of phytoconstituents such as polyphenols (240–290 nm) and flavonoids (420 nm), which likely mediated the reduction, stabilization, and capping of ZnONPs (Fig. 2a).

Fourier Transform Infrared Spectroscopy analysis of ZnONPs

FTIR spectrum of synthesized ZnONPs showed a broad band at 3407.18 cm^{-1} was related to the N–H stretching of primary amines, while the intense peak at 1560.17 cm^{-1} corresponded to the N–H bending of amines and C=C stretching of cyclic alkenes. The peak at 1320.55 cm^{-1} was attributed to C–F, S=O, and C–N stretching, indicating the presence of fluoro compounds, sulfone, and aromatic amine groups, respectively. The peak at 1030.76 cm^{-1} was associated with the C–O stretching of ethers and C–N stretching of amines, with smaller peaks at 883.51 cm^{-1} and 809.07 cm^{-1} attributed to the C–Cl stretching of halo compounds and C=C bending of alkenes.

The comparative FTIR spectrum of *A. indica* leaf extract showed the broad band at 3293.32 cm^{-1} was due to O–H stretching of alcohols and carboxylic acids, N–H stretching of aliphatic primary amine and secondary amine, and C–H stretching of alkynes. The peaks at 2919.99 cm^{-1} and 2851.08 cm^{-1} were attributed to O–H stretching of carboxylic acids, N–H stretching of amines and C–H stretching of alkanes. The peak at 1722.48 cm^{-1} was attributed to the C=O stretching, indicating carbonyl groups from aldehydes and ketones. The broad peak at 1606.55 cm^{-1} corresponded to the C=C stretching of alkenes and N–H bending of amines. The peak at 1361.64 cm^{-1} indicated S=O stretching of sulfonates and O–H bending of phenols. Peaks at 1237.06 cm^{-1} and 1157.25 cm^{-1} corresponded to

C–O and C–N stretching of ethers and amines, with the strong peak at 1030.47 cm^{-1} associated with S=O stretching of sulfoxides and C–O stretching of ethers. The peak at 816.23 cm^{-1} was observed due to C–Cl stretching in halo compounds and C=C bending of alkenes (Fig. 2b).

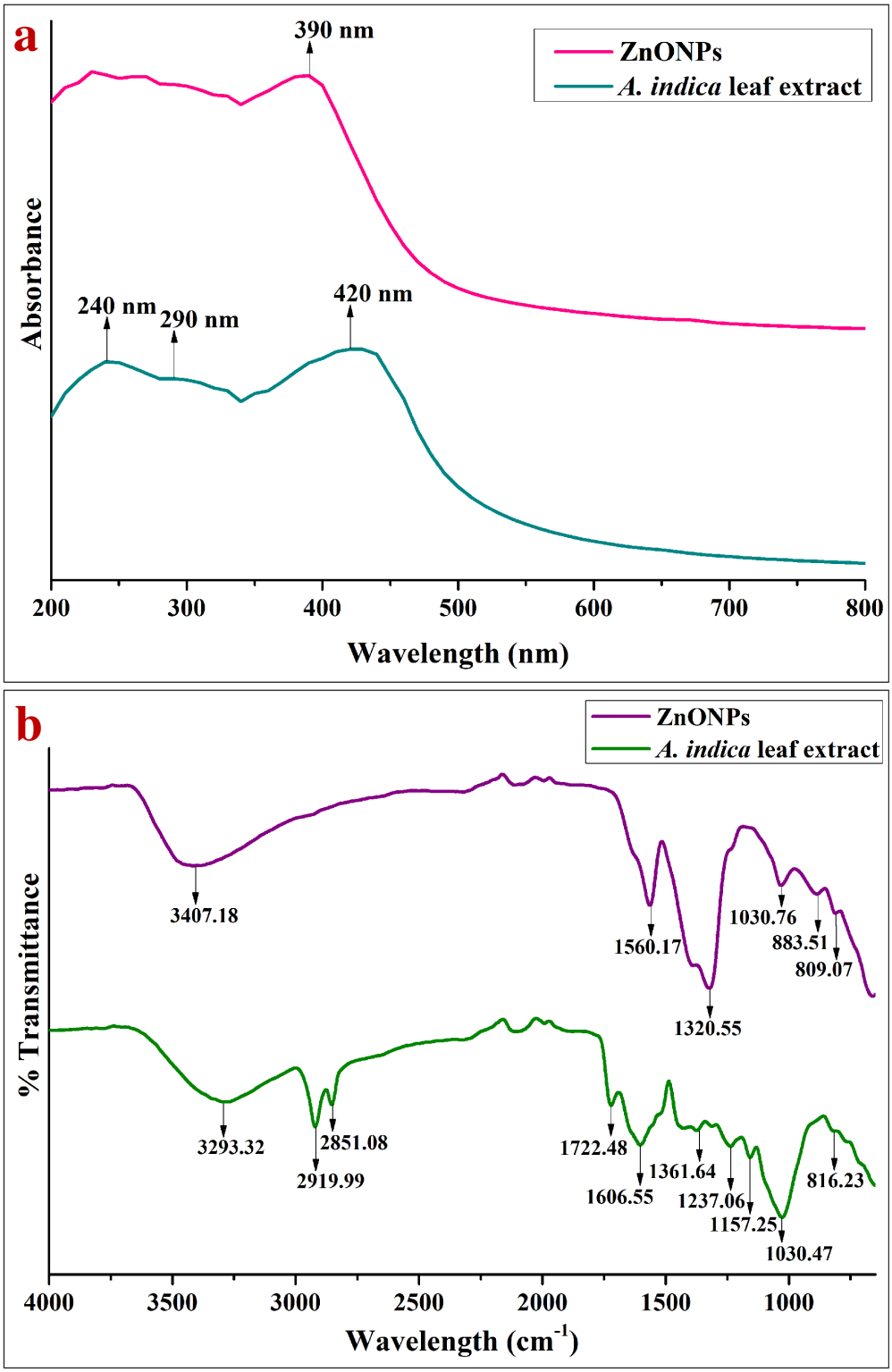


Fig. 2. Spectroscopic representation of green synthesized ZnONPs and leaf extract of *Azadirachta indica*. **(a)** UV-Visible spectra, **(b)** Fourier transform infrared spectra.

Field Emission Scanning Electron Microscopy and Energy Dispersive X-ray Spectroscopy analysis of ZnONPs

FESEM showed predominantly spherical morphology of green synthesized ZnONPs, with some degree of aggregation (Fig. 3a, 3b). EDX analysis identified three characteristic zinc (Zn) peaks at 1 keV, 8.63 keV, and 9.6 keV, alongside an oxygen (O) peak at 0.5 keV. The elemental analysis revealed 83.07% Zn and 16.93% O as the primary constituents in the synthesized ZnONPs (Fig. 3c).

X-ray Diffraction analysis of ZnONPs

The structural phase and crystallinity of the synthesized ZnONPs were characterized using XRD. The diffractogram (Fig. 3d) exhibited eight distinct, high-intensity peaks at 2θ = 31.86°, 34.50°, 36.32°, 47.85°, 56.67°, 62.97°, 68.05°, and 69.17°. These peaks were indexed to the (100), (002), (101), (102), (110), (103), (112), and (201) crystalline planes, respectively, identifying hexagonal wurtzite phase in excellent agreement with JCPDS card No. 36-1451. The average crystallite size of the synthesized ZnONPs, calculated via the Debye-Scherrer equation, was determined to be 12.28 nm (Table S1).

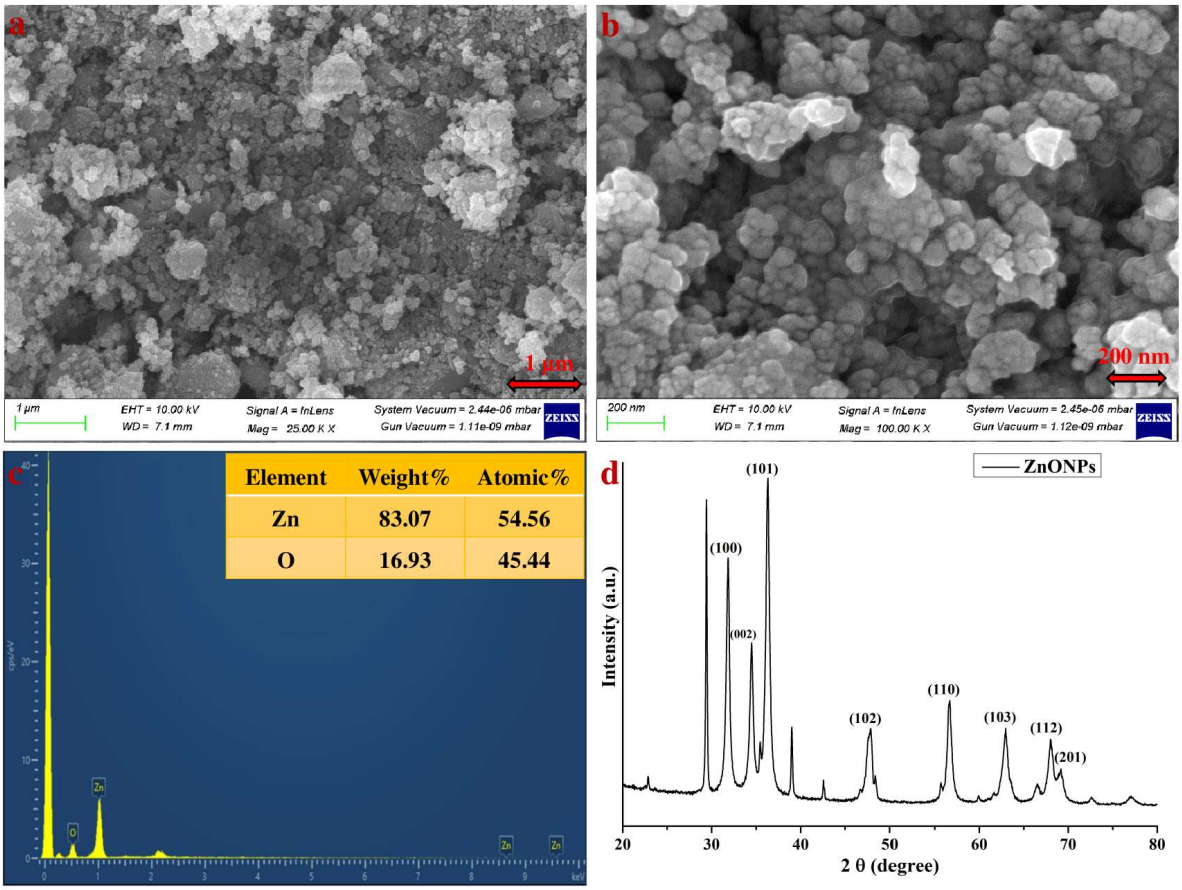


Fig. 3. Morphological and structural characterization of ZnONPs **(a-b)** Field emission scanning electron microscopy of ZnONPs at 1 µm and 200 nm, **(c)** Energy dispersive X-ray spectroscopy of ZnONPs, **(d)** X-ray diffraction of ZnONPs.

Transmission Electron Microscopy analysis of ZnONPs

The TEM analysis of the synthesized ZnONPs exhibited a spherical shape with uniform distribution, with mean particle sizes of 17.5 nm. The size distribution histograms were moderately skewed toward smaller particle sizes (Fig. 4).

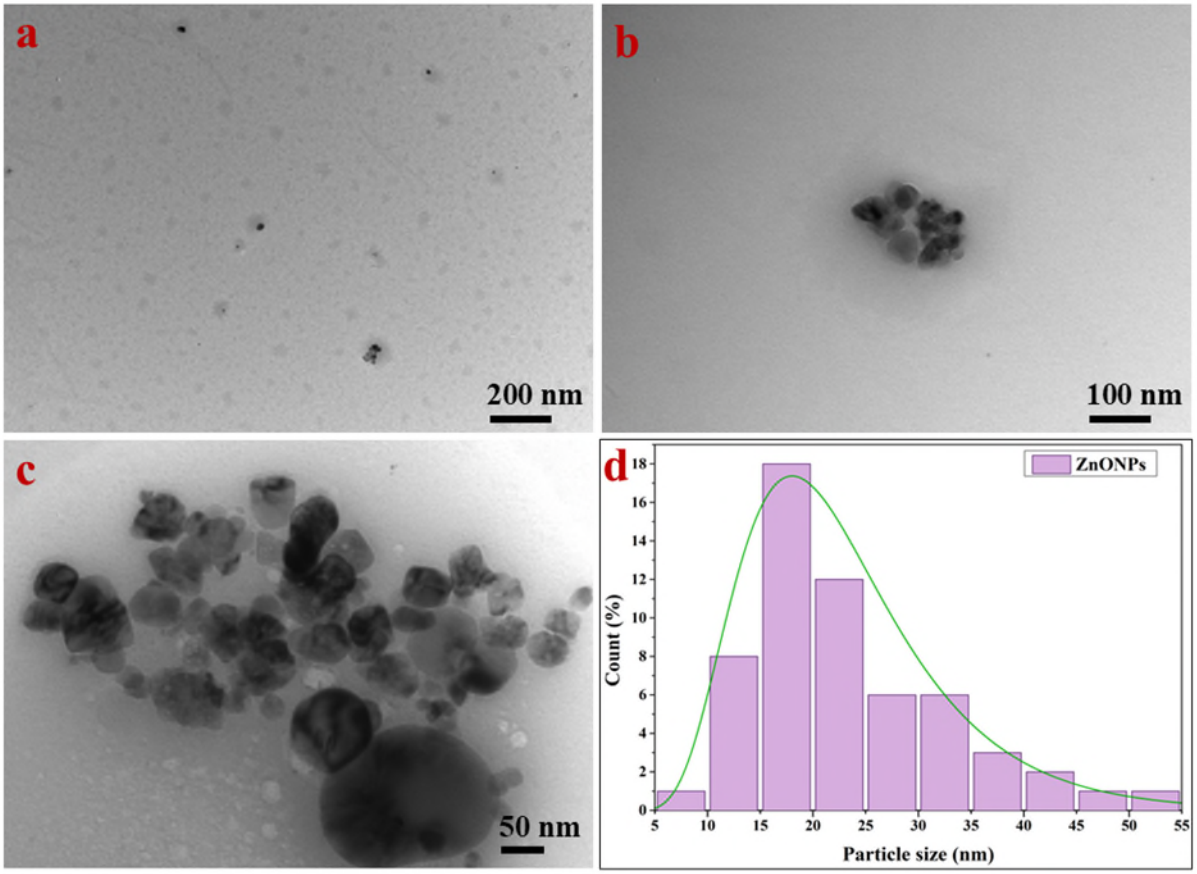


Fig. 4. Transmission electron microscopy of ZnONPs at **(a)** 200 nm, **(b)** 100 nm, **(c)** 50 nm, **(d)** Particle size distribution.

In vitro antifungal analysis of ZnONPs

The synthesized ZnONPs were evaluated for their *in vitro* antifungal activity. ZnONPs demonstrated concentration-dependent inhibition of fungal growth across all four tested phytopathogenic fungi (Fig. 5). After 7 days of incubation, significant antifungal activity was observed at concentrations ranging from 10 to 2000 mg L^{-1}. The inhibition zones increased with higher ZnONPs concentrations. ZnONPs showed inhibition percentages ranging from 47–100% for *R. solani*, 0–100% for *S. sclerotiorum*, 11–100% for *C. falcatum*, and 5–80% for *C. gloeosporioides*. While the negative control showed no inhibition, the positive control consistently achieved 100% suppression (Fig. S1). *R. solani* and *S. sclerotiorum* exhibited higher inhibition and were more susceptible to the synthesized ZnONPs compared to *C. falcatum* and *C. gloeosporioides* across all concentrations and incubation periods (Fig. S2).

Heatmap analysis corroborated these findings, confirming enhanced fungal suppression at higher concentrations, with higher doses of ZnONPs approaching the inhibition levels of the positive control (Fig. 6). The EC_{50} values for the ZnONPs were 23.12 mg L^{-1} (*R. solani*), 273.9 mg L^{-1} (*S. sclerotiorum*), 393.4 mg L^{-1} (*C. falcatum*), and 512.4 mg L^{-1} (*C. gloeosporioides*) (Fig. 7).

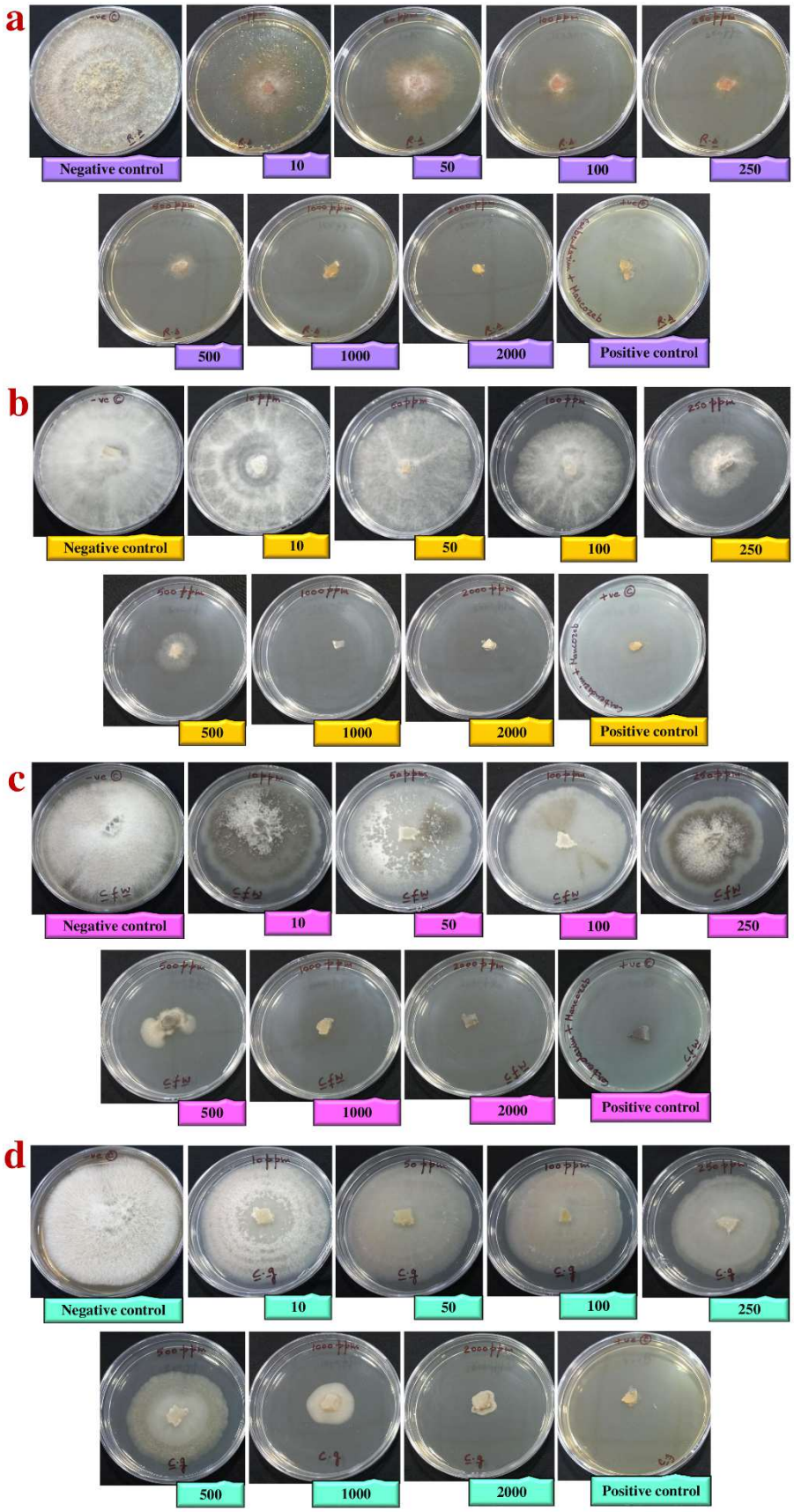


Fig. 5. *In vitro* antifungal activity of ZnONPs (10–2000 mg L^{-1}) showing the zone of inhibition against four phytopathogenic fungi: **(a)** *Rhizoctonia solani*, **(b)** *Sclerotinia sclerotiorum*, **(c)** *Colletotrichum falcatum*, and **(d)** *C. gloeosporioides*.

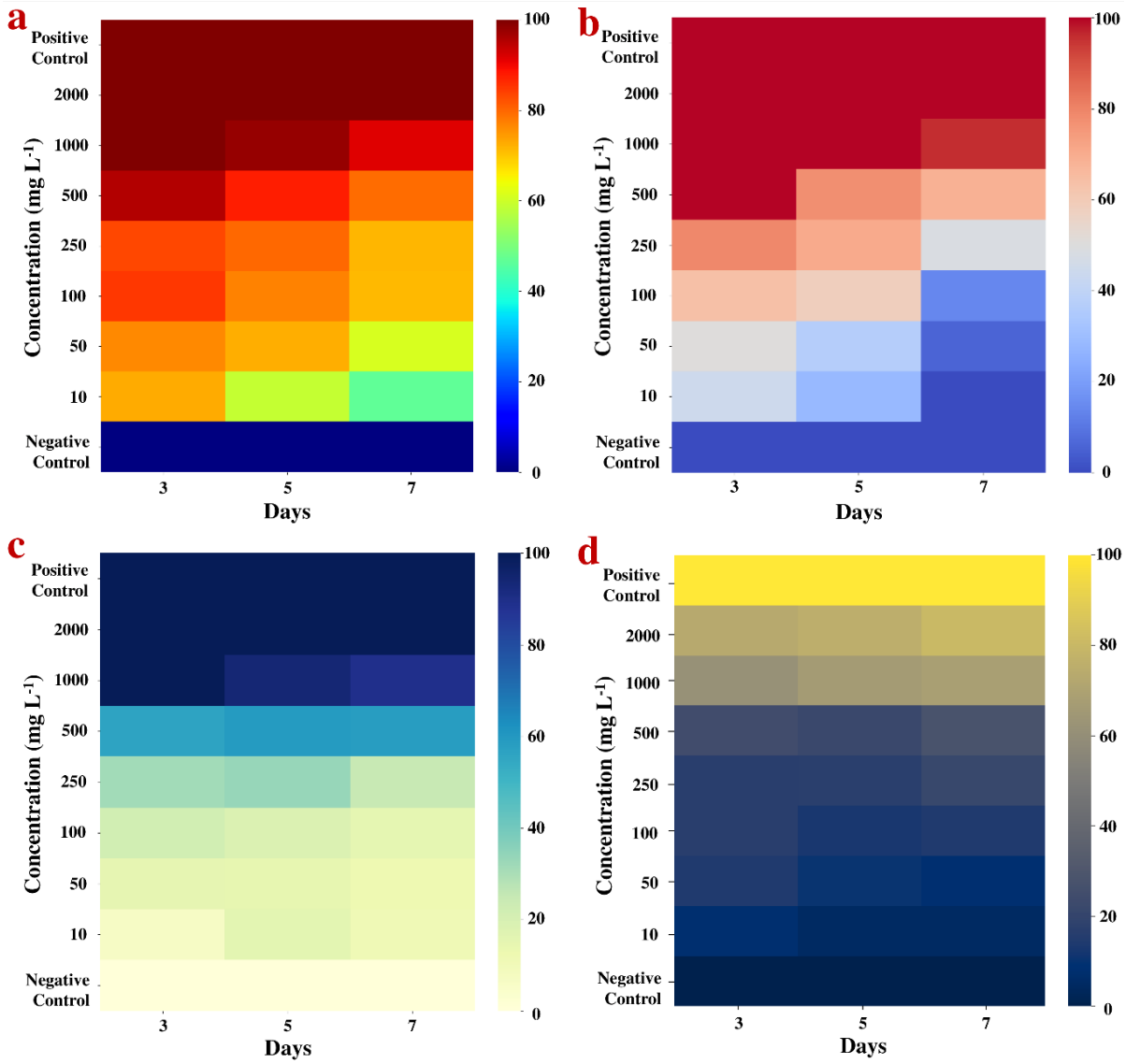


Fig. 6. Heat maps illustrating the percentage inhibition of fungal growth at different ZnONPs concentrations (10–2000 mg L^{-1}) after 3,5, and 7 days post-inoculation for: **(a)** *Rhizoctonia solani*, **(b)** *Sclerotinia sclerotiorum*, **(c)** *Colletotrichum falcatum*, and **(d)** *C. gloeosporioides*.

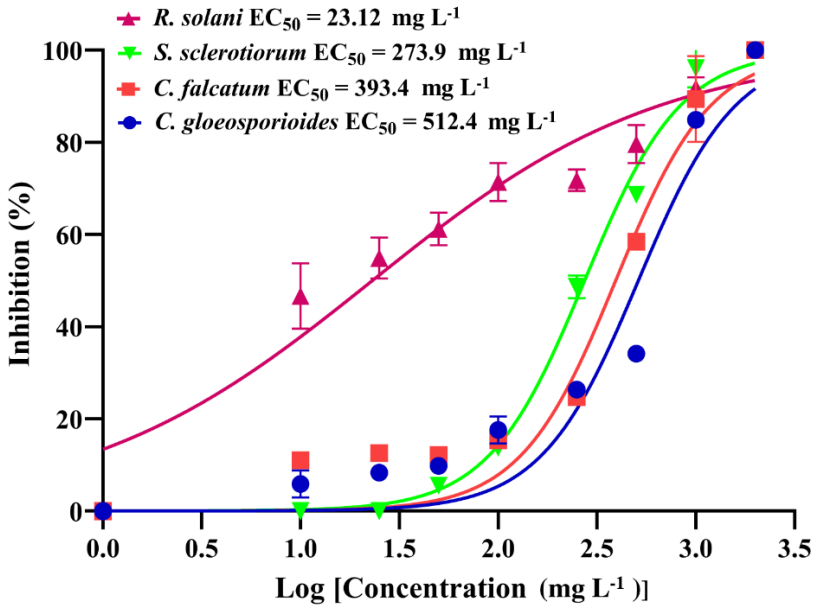


Fig. 7. Dose response (EC_{50}) curve of ZnONPs (mg L^{-1}) against *Rhizoctonia solani*, *Sclerotinia sclerotiorum*, *Colletotrichum falcatum*, and *C. gloeosporioides*.

Detached fruit and leaf assays

Evaluation of ZnONPs against *C. gloeosporioides* on *M. indica*

The efficacy of synthesized ZnONPs against *C. gloeosporioides* was assessed using a detached fruit assay on *M. indica* fruits. Initial infection symptoms appeared by day 2 post-inoculation, progressing to severe rot in controls by day 7. Treatment with ZnONPs progressively reduced lesion diameters from 15.96 to 11.54 mm at 500 to 2000 mg L^{-1}, achieving 73.95–81.16% disease inhibition and limiting disease infected area to 18.84–26.05% of the fruit surface. ZnONPs treatment showed concentration-dependent efficacy, with lesion scores decreasing from 1.88 to 1.33 at 500–2000 mg L^{-1}. Control groups showed expected results: control infected fruits displayed the highest score of 5, with severe disease infection and no disease inhibition, while untreated fruits maintained perfect integrity with a lesion score of 0 and no disease incidence throughout the observation period (Fig. 8, 9; Table S2).

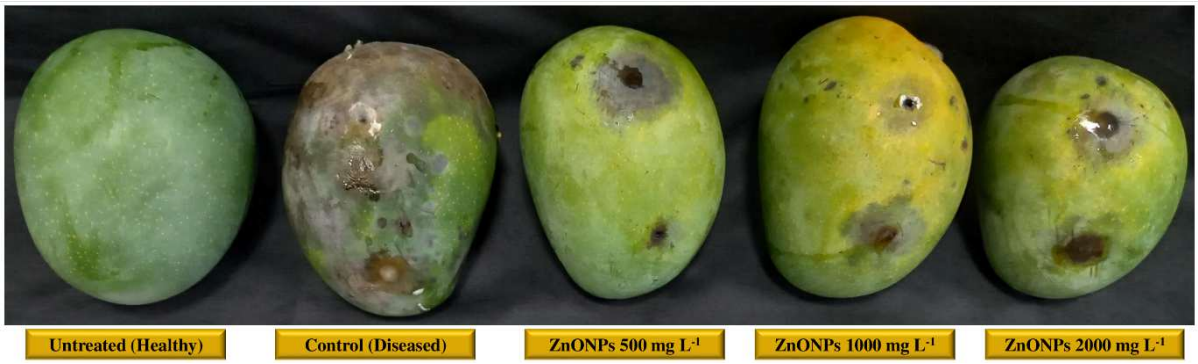


Fig. 8. Detached fruit assay showing the effect of ZnONPs (mg L^{-1}) on anthracnose development by *Colletotrichum gloeosporioides* on *Mangifera indica.* Images represent typical disease symptoms at 7 days post-inoculation.

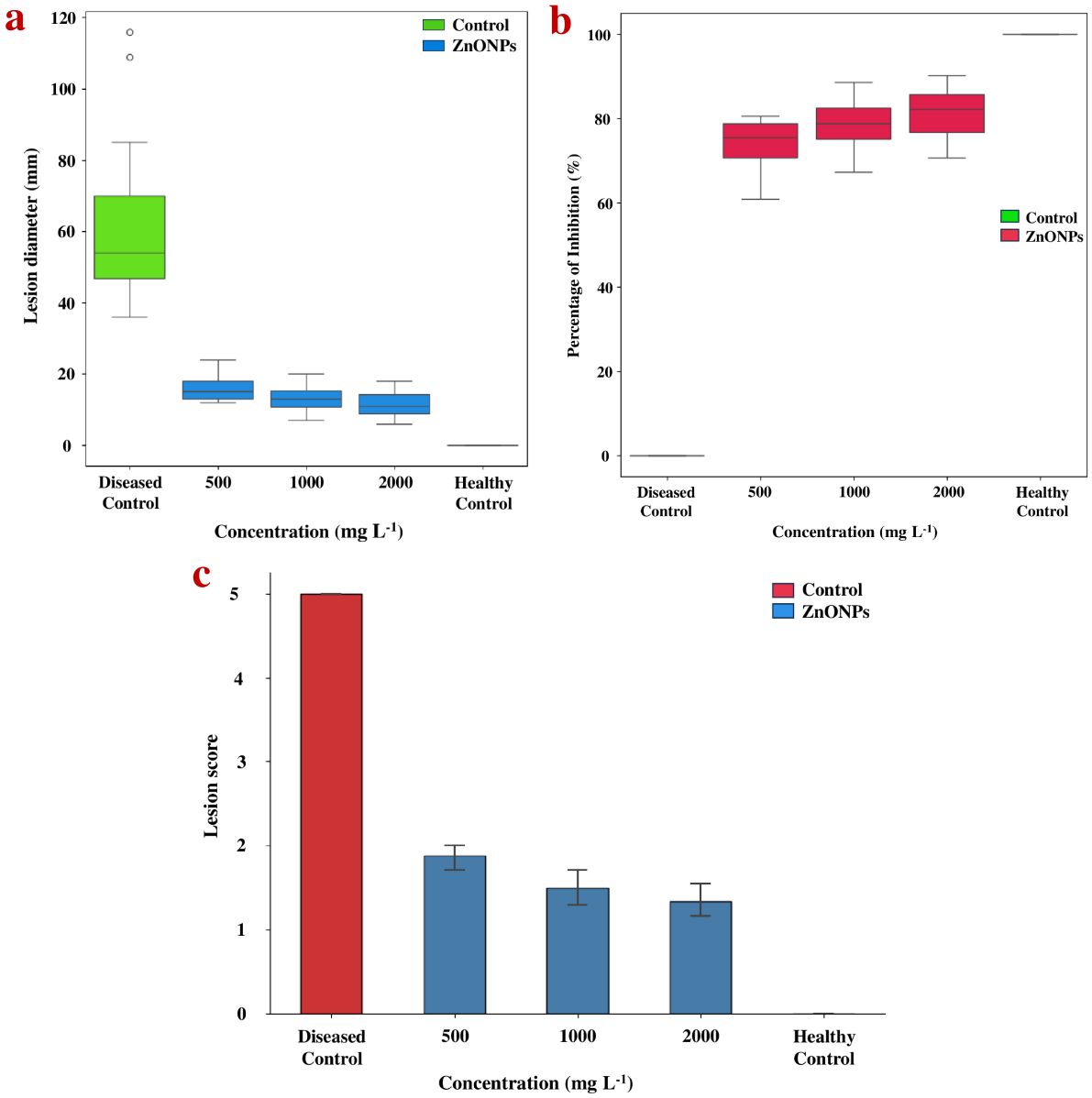


Fig. 9. Graphical representation of the detached fruit assay of ZnONPs (mg L^{-1}) against *Colletotrichum gloeosporioides* on *Mangifera indica* **(a)** Lesion diameter (mm), **(b)** Percentage of inhibition (%), and **(c)** Lesion score (error bars indicate the standard error).

Evaluation of ZnONPs against *R. solani* on *Z. mays*

The efficacy of ZnONPs against *R. solani* was evaluated using a detached leaf assay on *Z. mays* leaves. Initial infection symptoms appeared by day 2 post-inoculation, progressing to severe rot in the infected control by day 5. Lesion diameters on ZnONPs treated leaves significantly decreased with increasing concentrations, ranging from 5.0 mm at 500 mg L^{-1} to 0 mm at 2000 mg L^{-1}. Corresponding diseased leaf areas and PDI were reduced from 8.33% to 0%, while PDR significantly increased with concentration, reaching from 69.39% to 100%. In contrast, the infected control exhibited a lesion diameter of 16.33 mm, 100% diseased leaf area, a PDI of 27.22%, and 0% PDR, indicating severe disease progression. The untreated (healthy) control remained disease-free, with no visible lesions or signs of infection. Lesion scores, assessed on a 0–9 scale, were reduced from 3.22 to 0 across the 500 to 2000 mg L^{-1} concentration range. The untreated remained disease-free, with no lesions or disease incidence (Fig. 10, 11; Table S3).

Evaluation of ZnONPs against *R. solani* on *O. sativa*

ZnONPs significantly reduced *R. solani* infection in *O. sativa* leaves in a concentration-dependent manner. Lesion diameters on ZnONPs treated leaves decreased significantly with increasing concentrations, ranging from 3.0 mm at 500 mg L^{-1} to complete inhibition (0 mm) at 2000 mg L^{-1}. Correspondingly, diseased leaf areas and PDI were reduced from 5.0% to 0%, while PDR increased significantly, reaching from 73.53% to 100%. Diseased leaf areas and PDI were reduced to 0%, and PDR increased with concentration, reaching 100% at 2000 mg L^{-1}. In contrast, the infected control exhibited a lesion diameter of 11.33 mm, a 100% diseased leaf area, a PDI of 18.89%, and 0% PDR, indicating severe infection. The untreated (healthy) control remained disease-free, maintaining baseline conditions with no lesions or fungal growth. Lesion scores, evaluated on a 0–9 scale, were reduced from 2.89 to 0 across the concentration range of 500 to 2000 mg L^{-1}. In comparison, the infected control had a lesion score of 9. The untreated control remained unaffected, confirming optimal conditions with no disease symptoms (Fig. 10, 11; Table S4).

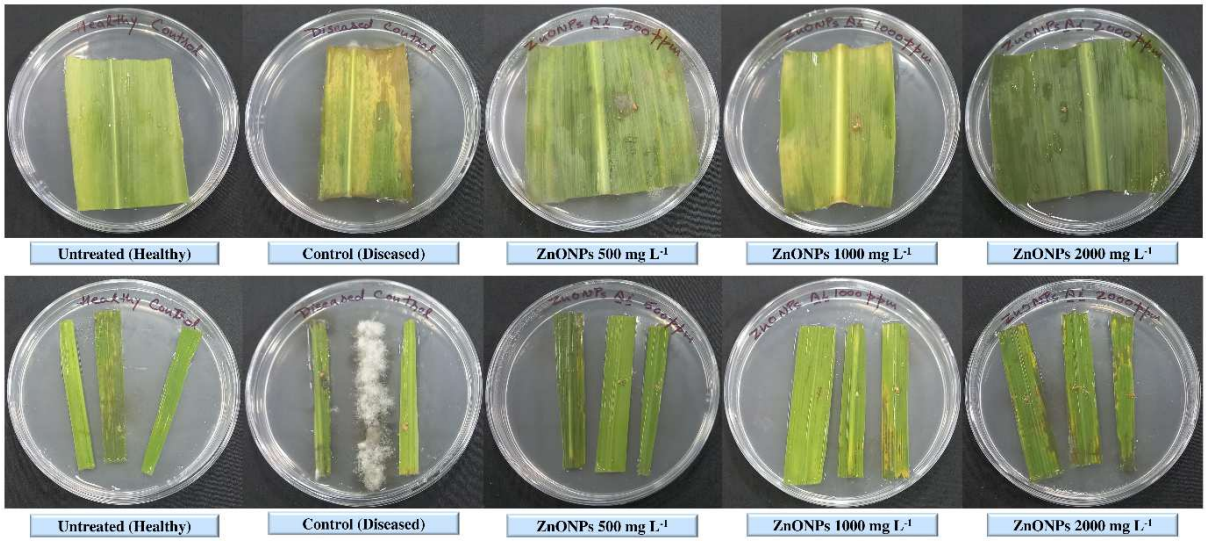


Fig. 10. Detached leaf assays demonstrating ZnONPs (mg L^{-1}) mediated disease suppression of *Rhizoctonia solani* on leaves of *Zea mays* (upper row) and *Oryza sativa* (lower row).

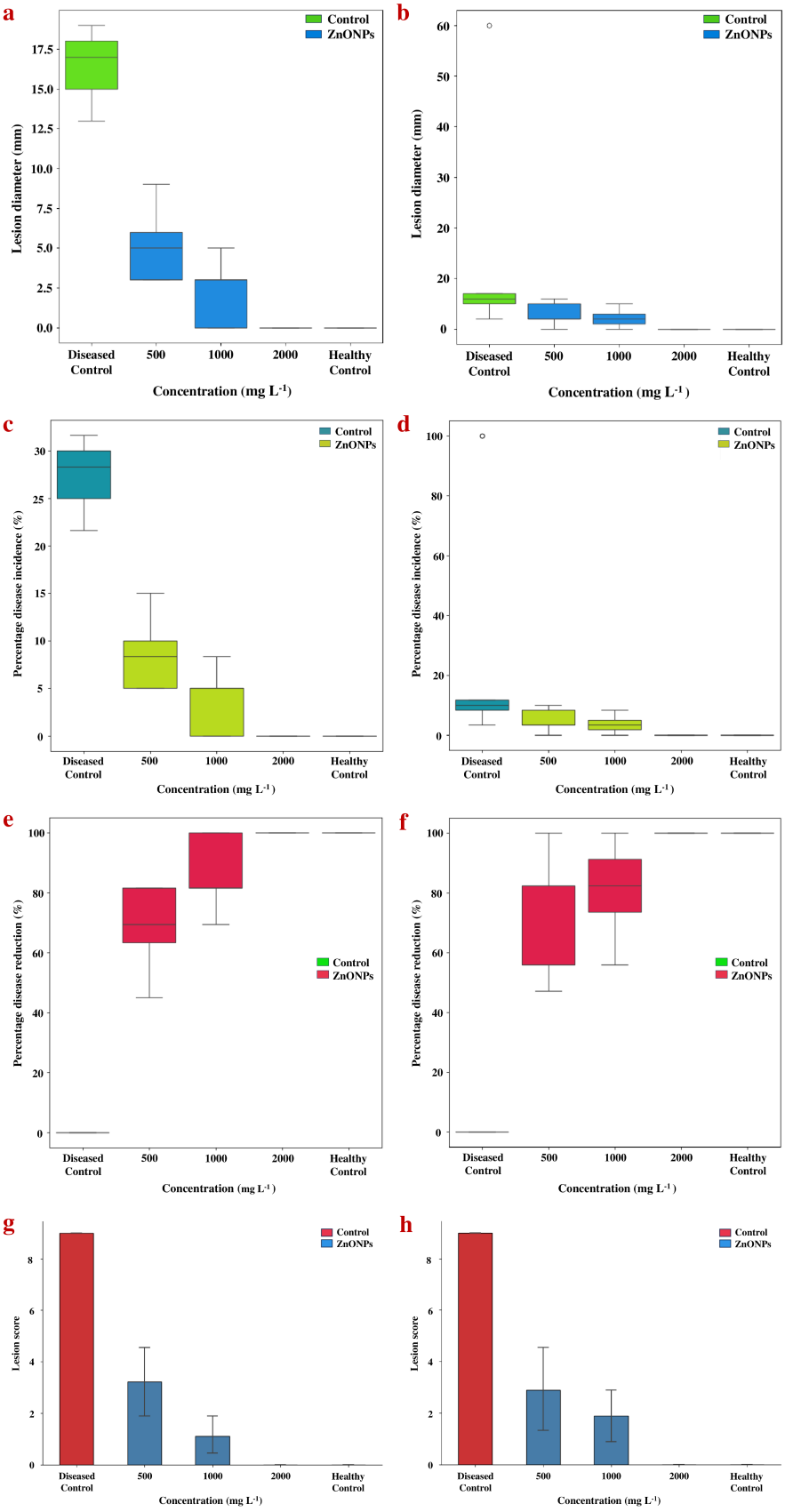


Fig. 11. Graphical representation of the detached leaf assay of ZnONPs (mg L^{-1}) against *Rhizoctonia solani* on *Zea mays* (first column) and *O. sativa* (second column) **(a, b)** Lesion diameter (mm), **(c, d)** Percentage of disease incidence (%), **(e, f)** Percentage of disease reduction (%), **(g, h)** Lesion score (error bars indicate the standard error).

Effect of ZnONPs seed nanopriming on early seedling growth under greenhouse conditions

Effect of ZnONPs nanopriming on *T. aestivum*

The seeds of *T. aestivum* showed 100% germination at different concentrations of ZnONPs, alongwith unprimed and hydroprimed seeds, which served as controls. Root length, shoot length, and biomass increased at 100 mg L^{-1} ZnONPs compared to unprimed and hydroprimed controls. The number of roots in *T. aestivum* plants was increased at both the concentrations of ZnONPs (100 and 500 mg L^{-1}) as compared to controls (Fig. 12).

Effect of ZnONPs nanopriming on *C. arietinum*

The seeds of *C. arietinum* showed 100% germination at 100 mg L^{-1} concentration of ZnONPs. The germination percentage was reduced to 88.88% at 500 mg L^{-1}, similar to the unprimed and hydroprimed controls. Primary root length, secondary root length, and shoot length increased at both the ZnONPs concentration as compared to the controls. The maximum enhancement was observed at 100 mg L^{-1} of ZnONPs. The number of secondary roots was also increased at 100 mg L^{-1}, while 500 mg L^{-1} treatment of ZnONPs was comparable to the hydroprimed control. Fresh and dry root and shoot weight was also increased at both ZnONPs concentrations compared to the controls (Fig. 13).

Effect of ZnONPs nanopriming on *S. lycopersicum*

The seeds of *S. lycopersicum* showed the highest germination at 100 mg L^{-1} of ZnONPs. While the percentage of germination at 500 mg L^{-1} was comparable to the hydroprimed control and lowest at the unprimed control. Most of the morphological traits, including primary root length, secondary root length, shoot length, fresh and dry weight of root and shoot, showed the maximum enhancement at 100 mg L^{-1} of ZnONPs, while 500 mg L^{-1} was approximately comparable to the hydroprimed control and higher than the unprimed control. The number of secondary roots was increased at both concentrations of ZnONPs, similar to the hydroprimed control and higher than the unprimed control (Fig. 14).

Effect of ZnONPs nanopriming on *B. nigra*

The seeds of *B. nigra* showed germination only at 100 mg L^{-1} of ZnONPs, concentration while no germination was observed at 500 mg L^{-1}. The highest percentage of germination was observed at 100 mg L^{-1} as compared to the unprimed and hydroprimed controls. All morphological traits, including primary root length, secondary root length, shoot length, number of secondary roots, fresh and dry weight of root and shoot, showed the maximum enhancement at 100 mg L^{-1} as compared to the control (Fig. 15).

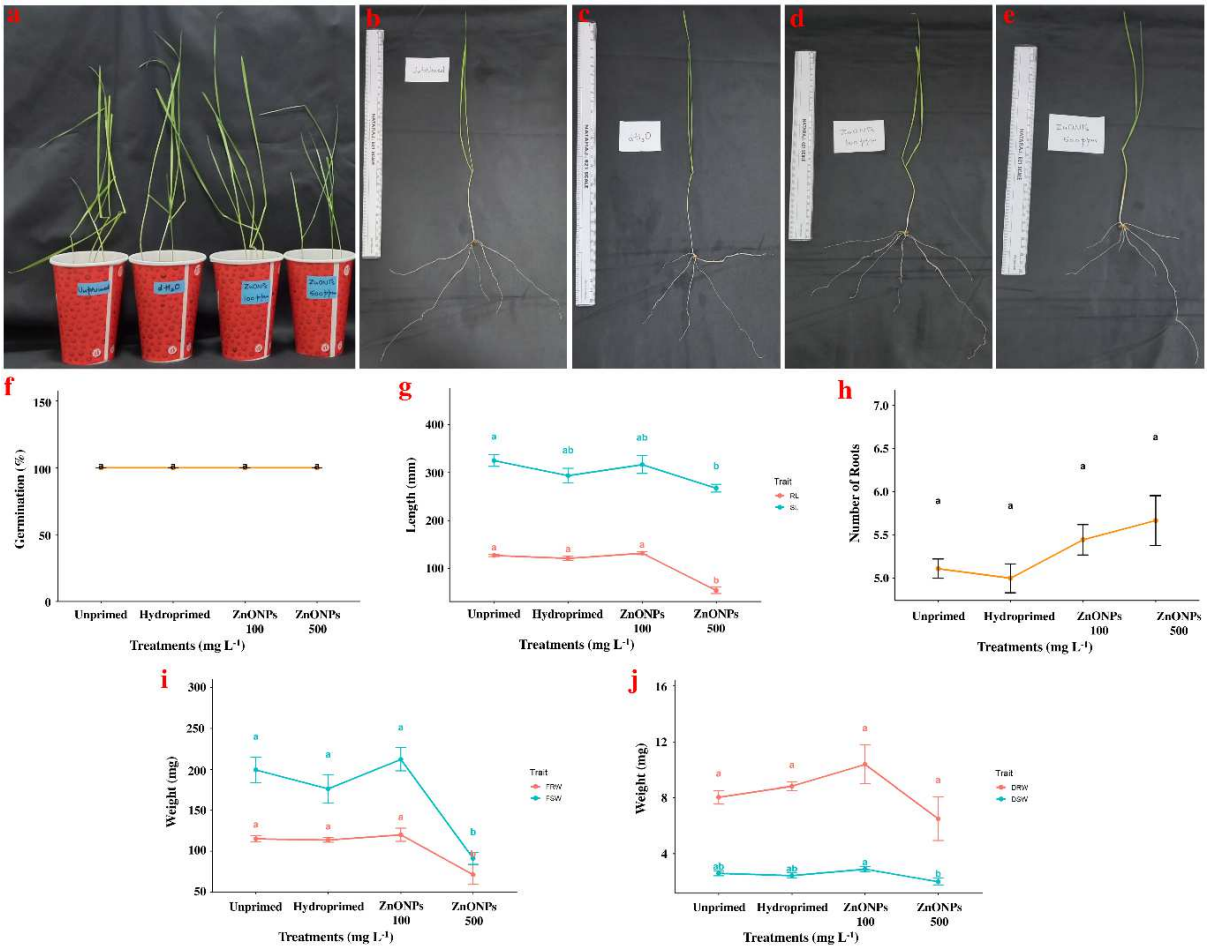


Fig. 12. Effect of ZnONPs nanopriming (100 and 500 mg L^{-1}) on *Triticum aestivum*. **(a)** Early seedling growth under greenhouse conditions. Shoot and root growth under different treatments **(b)** Unprimed, **(c)** Hydroprimed, **(d)** ZnONPs at 100 mg L^{-1}, **(e)** ZnONPs at 500 mg L^{-1}. The scale bar represents seedling length in millimeters. Line plot analysis of the effect of ZnONPs on different morphological traits **(f)** Germination (%), **(g)** Root length (mm), Shoot length (mm), **(h)** Number of roots, **(i)** Fresh root weight (mg), Fresh shoot weight (mg) **(j)** Dry root weight (mg), Dry shoot weight (mg). Data are presented as mean ± standard error (SE) based on nine replicates per treatment. Different lowercase letters above the data points indicate significant ($p \leq 0.05$) differences among treatments.

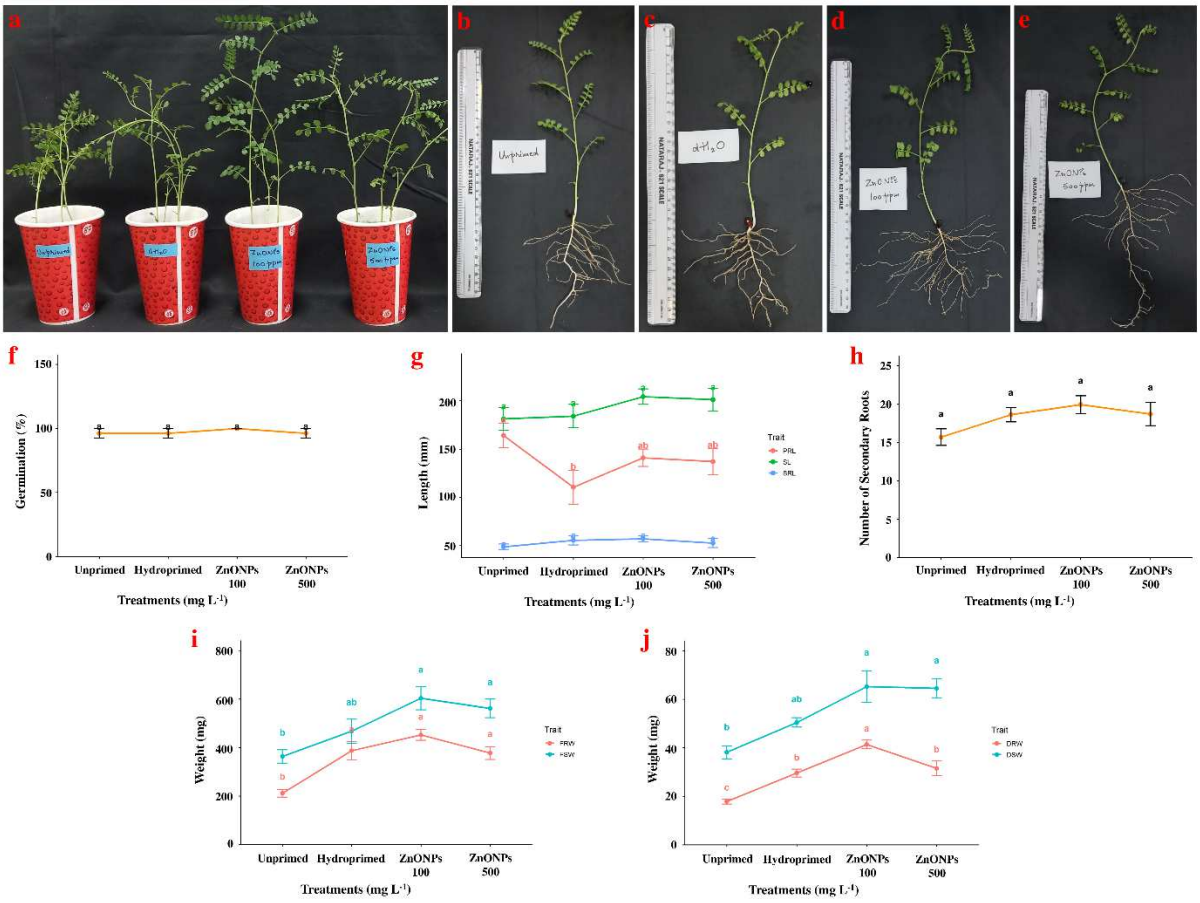


Fig. 13. Effect of ZnONPs nanopriming (100 and 500 mg L^{-1}) on *Cicer arietinum*. **(a)** Early seedling growth under greenhouse conditions. Shoot and root **(b)** Unprimed, **(c)** Hydroprimed, **(d)** 100 mg L^{-1}, **(e)** 500 mg L^{-1} (nanoprimed). Line plot analysis of the effect of ZnONPs on different morphological traits **(f)** Germination (%), **(g)** Primary root length (mm), Secondary root length (mm), Shoot length (mm), **(h)** Number of secondary roots, **(i)** Fresh root weight (mg), Fresh shoot weight (mg) **(j)**, Dry root weight (mg), Dry shoot weight (mg). Data are presented as mean ± standard error (SE) based on nine replicates per treatment. Different lowercase letters above the data points indicate significant ($p \leq 0.05$) differences among treatments.

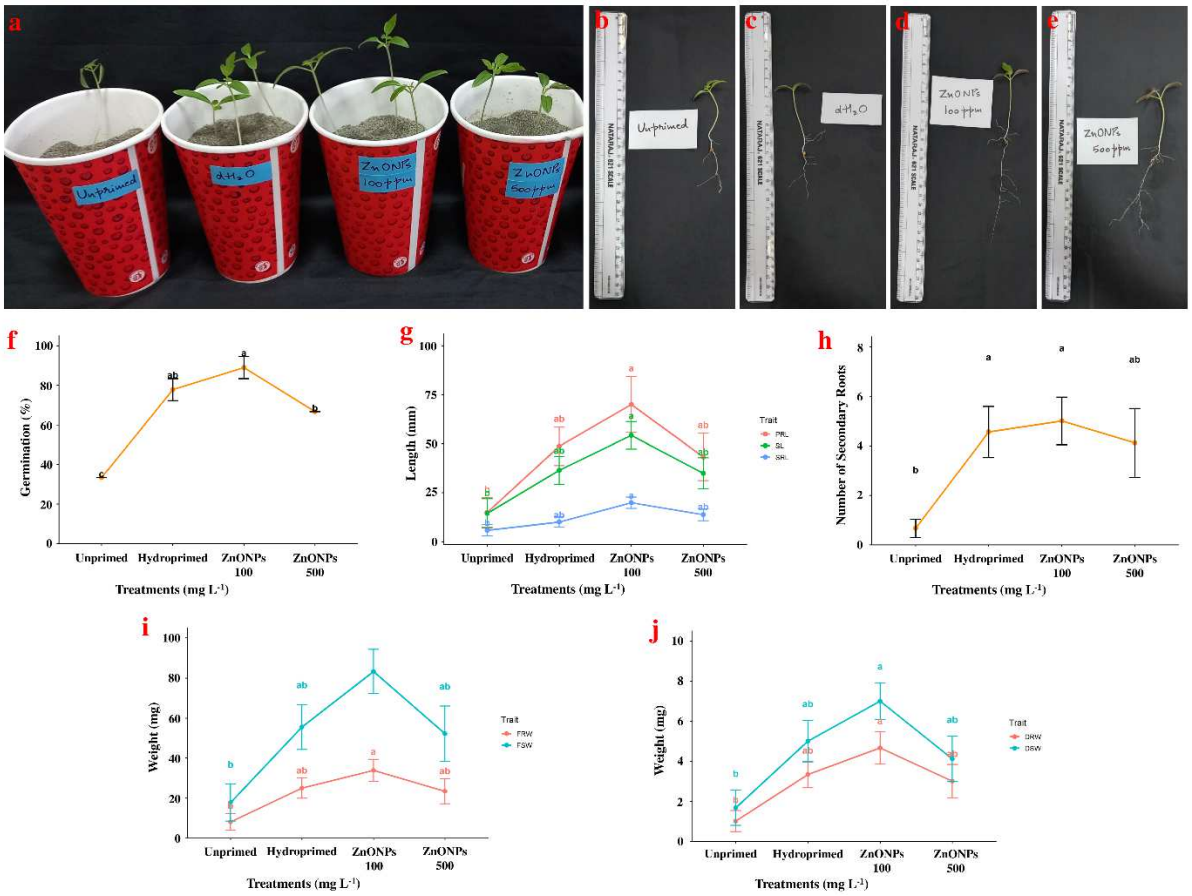


Fig. 14. Effect of ZnONPs nanopriming (100 and 500 mg L^{-1}) on *Solanum lycopersicum*. **(a)** Early seedling growth under greenhouse conditions. Shoot and root **(b)** Unprimed, **(c)** Hydroprimed, **(d)** 100 mg L^{-1}, **(e)** 500 mg L^{-1} (nanoprimed). Line plot analysis of the effect of ZnONPs on different morphological traits **(f)** Germination (%), **(g)** Primary root length (mm), Secondary root length (mm), Shoot length (mm), **(h)** Number of secondary roots, **(i)** Fresh root weight (mg), Fresh shoot weight (mg) **(j)**, Dry root weight (mg), Dry shoot weight (mg). Data are presented as mean ± standard error (SE) based on nine replicates per treatment. Different lowercase letters above the data points indicate significant ($p \leq 0.05$) differences among treatments.

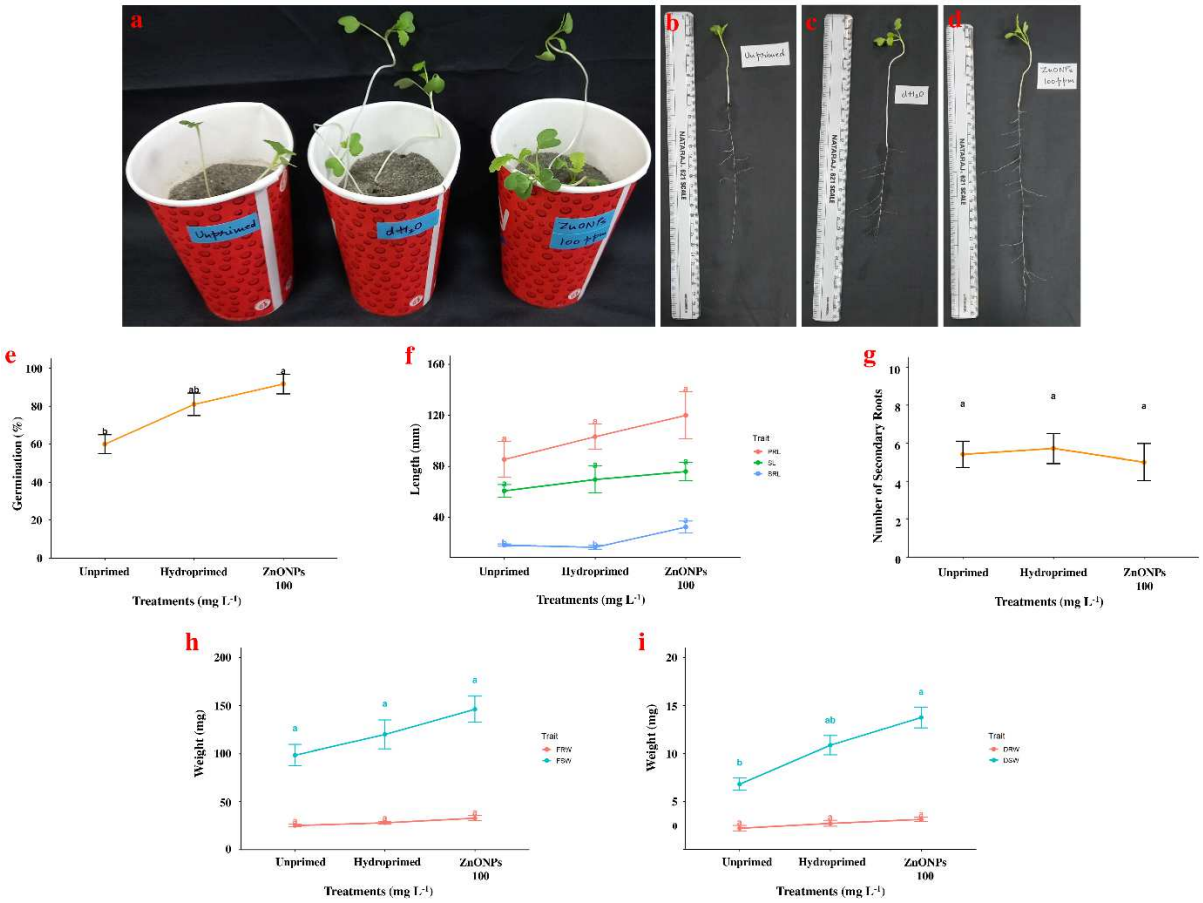


Fig. 15. Effect of ZnONPs nanopriming (100 mg L^{-1}) on *Brassica nigra* **(a)** Early seedling growth under greenhouse conditions. Shoot and root **(b)** Unprimed, **(c)** Hydroprimed, **(d)** 100 mg L^{-1} (nanoprimed). Line plot analysis of the effect of ZnONPs on different morphological traits **(e)** Germination (%), **(f)** Primary root length (mm), Secondary root length (mm), Shoot length (mm), **(g)** Number of secondary roots, **(h)** Fresh root weight (mg), Fresh shoot weight (mg) **(i)**, Dry root weight (mg), Dry shoot weight (mg). Data are presented as mean ± standard error (SE) based on nine replicates per treatment. Different lowercase letters above the data points indicate significant ($p \leq 0.05$) differences among treatments.

Discussion

The green synthesis approach using *A. indica* leaf extract produced ZnONPs with reproducible physicochemical characteristics, supporting the feasibility of plant-mediated synthesis as an alternative to conventional chemical routes [65]. The phytochemical constituents of *A. indica* leaf extract, including flavonoids and phenolic compounds, facilitated the reduction of Zn^{2+} ions, leading to the synthesis of ZnONPs and also functioned as effective capping and stabilizing agents [37]. This study successfully demonstrated the green synthesis of stable and crystalline ZnONPs by using higher precursor concentration and also advances its biological applications. The green synthesis of ZnONPs was facilitated by OH and COOH groups present in the plant leaf extract. The OH group from the phytochemicals acted as reducing agents, converting Zn^{2+} ions into ZnONPs through a redox reaction [66]. The stabilization of ZnONPs occurred through electrostatic and steric interactions, preventing agglomeration and ensuring the stability of the synthesized ZnONPs [67]. The small and broad absorption peak of the synthesized ZnONPs was attributed to their small particle size [68]. Singh & Kaushik (2019) [69] and Yadeta & Lealem (2024) [70] reported the absorbance peak at 368 nm and 370 nm for the synthesized ZnONPs using *A. indica*. The absorption peaks observed at 240 nm indicate the presence of phenolic compounds contributes to the reducing and stabilizing properties of *A. indica* for

ZnONPs synthesis [71]. The peaks at 290 nm revealed the presence of flavonoids, while the peaks at 420 nm indicated the presence of carotenoids that contribute to stabilizing effects [72].

Dodoo-Arhin et al. (2021) [73] reported that the FTIR fingerprint bands observed below 1000 cm^{-1} are characteristic of the Zn-O bond, representing inter-atomic vibrations specific to the metal zinc, as metal-related bands typically appear in this region [74]. The FTIR analysis of ZnONPs revealed significant shifts in spectral peaks of the synthesized nanoparticles compared to *A. indica* leaf extracts [37]. These functional groups were mainly attributed to flavonoids, terpenoids, tannins, and saponins present in the leaf extract [75]. These functional groups played a critical role in the efficient reduction of Zn^{2+} ions into ZnONPs and enhanced their stability [76].

The FESEM analysis of ZnONPs exhibited a spherical shape across different magnifications, indicating that the bioactive compounds in *A. indica* effectively controlled nanoparticle morphology. However, noticeable clustering and aggregation were also observed, indicating that the particles were not fully monodispersed with moderate size variation and the formation of aggregates. TEM analysis further confirmed the spherical shape of ZnONPs with narrow size distribution. The elemental profile of the synthesized ZnONPs, aligns closely with the expected stoichiometric values for zinc oxide. These findings validate the successful synthesis and phase purity of the synthesized ZnONPs [77]. The XRD pattern showed eight peaks of varying intensities for the synthesized ZnONPs. Additionally, the presence of some unassigned peaks suggests the occurrence of bioorganic phase crystallization on the surface of ZnONPs [78].

The selection of *T. aestivum, C. arietinum, S. lycopersicum*, and *B. nigra* was based on their agronomic relevance and their susceptibility to different fungal pathogens. *R. solani, S. sclerotiorum*, and *C. gloeosporioides* are established pathogens of the four selected crops, their inclusion in the antifungal assays allowed direct evaluation of ZnONPs effects against fungi of confirmed agronomic relevance [79–81]. Evaluating ZnONPs against pathogens that naturally infect these hosts provides a more realistic measure of their potential utility in crop protection. In this context, the *in vitro* antifungal analysis was performed and showed that percentage of inhibition was positively correlated with an increased concentration of ZnONPs. The antifungal activity of ZnONPs may involve multiple mechanisms previously reported for metal oxide nanoparticles, including membrane disruption and oxidative stress; however, these mechanisms were not directly examined in the present study [82, 83].

Detached fruit and leaf assays provide a semi *in vivo* system that enables controlled evaluation of host-pathogen interactions under laboratory conditions [84]. The direct inhibitory effect of the antifungal agents can be evaluated by measuring the reduction or suppression of disease symptoms in these assays [85]. In consequence, it provides disease response comparable to those observed in *in vivo* [86, 87].

ZnONPs demonstrated their antifungal efficacy against *C. gloeosporioides* on *M. indica*. Fruits treated with different concentration of ZnONPs and subsequently inoculated with *C. gloeosporioides* exhibited reduced symptoms of anthracnose disease (dark, sunken, circular lesions that cover most of the fruit) demonstrating dose-dependent inhibition of anthracnose symptoms [81]. As the concentration of ZnONPs increased, the lesion size and disease symptoms significantly decreased, with almost no lesions or symptoms at higher concentrations. The obtained results aligned with previous studies on the antifungal activity against *C. gloeosporioides* in detached fruit assays. Chowdappa et al. (2014) [60] reported 45.7% to 71.3% inhibition of *C. gloeosporioides* on the fruits of *M. indica* treated with a chitosan-AgNPs composite.

The synthesized ZnONPs also showed their efficacy against *R. solani* in a detached leaf assay on *Z. mays* and *O. sativa*. Leaves treated with ZnONPs, followed by inoculation with *R. solani*, showed reduced infection symptoms of BLSB in *Z. mays* and sheath blight in *O. sativa*. The obtained results were consistent with the previously reported literature. Chiranjeevi et al. (2018) [88] reported a PDR of 99% with 170 mg L^{-1} of AgNPs synthesized using *Trichoderma* and *Pseudomonas fluorescens*. Kora et

al. (2020) reported complete disease suppression (100% PDR) against various isolates of *R. solani* by utilizing 20 mg L^{-1} of green synthesized AgNPs using *O. sativa*. Divya et al. (2020) [89] also reported a 90% disease reduction of sheath blight using chitosan nanoparticles. Sahgal et al. (2024) [90] reported significant control of BLSB disease in *Z. mays* using *Pseudomonas* strains and demonstrated an efficient reduction of disease incidence from 25% to 38.33% compared to control treatments.

The inhibition of *R. solani* was attributed to the synthesized ZnONPs, which can easily penetrate the plant system due to their small size through stomata, wounds, and trichomes [91]. Stomata have been identified as an efficient route for nanoparticle uptake [92]. As monocots, *Z. mays* and *O. sativa* possess stomata on both leaf surfaces, potentially facilitating the rapid uptake of nanoparticles. Once they enter the plant, these nanoparticles may activate defence responses, thereby suppressing the growth of invading phytopathogens in addition to their inherent biocidal properties [87, 93].

Nanopriming influences early seedling development through changes in water uptake, hormonal balance, and micronutrient availability during imbibition, and these responses are known to vary widely among plant species [43, 46]. The interaction between nanoparticles and seeds is strongly governed by the permeability of the seed coat and the biochemical composition of the testa, which together determine nanoparticle entry and subsequent ion release to the embryo [94]. Metal oxide nanoparticles, including ZnONPs, can enhance germination by improving Zn availability, stimulating hydrolytic enzyme activity, and supporting early metabolic activation, but may also induce oxidative stress or disrupt metal homeostasis at higher concentrations [41, 45]. These physiological and structural differences provide a basis for expecting crop-specific responses to ZnONPs exposure and justify evaluating nanopriming effects across multiple crop groups.

ZnONPs nanopriming at 100 mg L^{-1} enhanced seed germination in all four types of plants. However, at 500 mg L^{-1}, germination was completely inhibited in *B. nigra*, whereas the other three crops continued to germinate. This suggests that *B. nigra* exhibits higher sensitivity to higher ZnONPs concentrations due to phytotoxic effects. Previous studies have also reported that species belonging to the *Brassicaceae* exhibit sensitivity to high concentration of metal nanoparticles [44, 46]. The increased germination in nanoprimed seeds, compared to unprimed and hydroprimed seeds, may be attributed to zinc-induced biochemical changes, including dormancy breaking, enzyme activation, and hydrolysis of inhibitors [95]. Additionally, zinc plays a critical role in carbohydrate and protein metabolism, contributing to synchronized germination and early seedling development. Geremew et al. (2023) [46] suggested that nanoparticles promote germination by enhancing water uptake and oxygen availability, facilitated by the creation of new seed coat pores.

ZnONPs significantly enhanced different morphological traits at 100 mg L^{-1} across all crops. Wlodarczyk & Smolinska (2022) [64] reported that the smaller ZnONPs significantly enhanced the germination in tomato seeds. Although, further research is required to determine the threshold concentration of ZnONPs that can be considered phytotoxic and to evaluate their potential environmental hazards, particularly regarding interactions with plant systems. The improvement of fresh and dry weight at 100 mg L^{-1} suggests that moderate treatment levels promote optimal root growth by supporting physiological processes such as cell division, elongation, and biomass partitioning. The elongation of radicles and plumules in the presence of ZnONPs is linked to zinc's role in synthesizing endogenous hormones such as auxins and gibberellins [44]. Earlier studies reported that ZnONPs exhibited a higher capacity for absorption and assimilation due to their nanoscale properties and slow, gradual release of Zn^{2+} ions [43, 47]. However, higher concentrations may adversely affect root growth, potentially due to stress-induced metabolic imbalance or reduced nutrient uptake efficiency [96]. While the integrated antifungal and nanopriming evaluation provides evaluation of green synthesized ZnONPs within relevant crop systems, the study does not address mechanistic pathways, long-term phytotoxicity. Together, the species-dependent results, concentration-specific responses, and nanoparticle stability highlight the need of field-scale validation and environmental outcomes, before considering broader

agricultural applications. Within these limitations, the results support further investigation of green synthesized ZnONPs for plant disease suppression and early seedling establishment. Future research should focus on understanding the precise molecular and physiological mechanisms of ZnONPs in plants, assessing their long-term effects, and ensuring their safe application for sustainable agriculture.

Conclusion

The present findings demonstrate that green-synthesized ZnONPs with defined physicochemical properties, including nanoscale size, high elemental purity, and stable dispersibility after powder recovery. The synthesized ZnONPs exhibit strong antifungal activity *in vitro* and in detached plant systems, along with concentration-dependent effects on early seedling growth following nanopriming. Importantly, the results also highlight clear species-specific and dose-dependent responses, including growth inhibition at higher concentrations. While these observations support further investigation of ZnONPs for plant protection and seed treatment applications, comprehensive studies addressing nanoparticle uptake, mode of action, long-term phytotoxicity, and field-level performance are required before broader agricultural deployment.

Acknowledgements

The authors are highly thankful to the Department of Science and Technology (DST-SERB file number EEQ/2018/001306) India, UP Government R & D scheme (2022), and the University Research Grant Scheme (URGS-URGS-DEV/URGS/2022-23/21) Chaudhary Charan Singh University, Meerut, U.P., India, for providing financial support for this research. The authors also thank the Institute Instrumentation Centre, IIT Roorkee, and the Central Research Facility, IIT Delhi, for providing instrumentation facilities for nanoparticle characterization.

Authors' contributions

J.S. and D.P. conceived the study and prepared the manuscript. J.S. carried out all the experimental work. J.S., A.K., and A.G. carried out the statistical and software analysis. All the authors read and approved the final manuscript.

Funding

This research did not receive any specific grant from funding agencies in the public, commercial, or not-for-profit sectors.

Availability of data and materials

Data will be made available on request.

Declarations

Ethics approval and consent to participate

Not applicable.

Consent for publication

Not applicable.

Competing interests

The authors declare no competing interests.

References

1. Savary S, Willocquet L, Pethybridge SJ, Esker P, McRoberts N, Nelson A. The global burden of pathogens and pests on major food crops. Nature ecology & evolution. 2019;3(3):430-9. https://doi.org/10.1038/s41559-018-0793-y
2. Gai Y, Wang H. Plant disease: A growing threat to global food security. Agronomy. 2024;14(8):1615. https://doi.org/10.3390/agronomy14081615
3. Pathak H, Mishra JP, Mohapatra T. Indian agriculture after independence. Indian Council of Agricultural Research, New Delhi. 2022;110(001):426. https://www.icar.org.in/sites/default/files/2023-02/Indian-Agriculture-after-Independence.pdf
4. Ajayi-Oyetunde OO, Bradley CA. *Rhizoctonia solani*: taxonomy, population biology and management of rhizoctonia seedling disease of soybean. Plant pathology. 2018;67(1):3-17. https://doi.org/10.1111/ppa.12733
5. Singh A, Singh NB, Hussain I, Singh H, Yadav V, Singh SC. Green synthesis of nano zinc oxide and evaluation of its impact on germination and metabolic activity of *Solanum lycopersicum*. Journal of biotechnology. 2016;233:84-94. https://doi.org/10.1016/j.jbiotec.2016.07.010
6. Derbyshire MC, Denton-Giles M. The control of sclerotinia stem rot on oilseed rape (*Brassica napus*): current practices and future opportunities. Plant Pathology. 2016;65(6):859-77. https://doi.org/10.1111/ppa.12517
7. Willbur J, McCaghey M, Kabbage M, Smith DL. An overview of the *Sclerotinia sclerotiorum* pathosystem in soybean: impact, fungal biology, and current management strategies. Tropical Plant Pathology. 2019;44(1):3-11. https://doi.org/10.1007/s40858-018-0250-0
8. Viswanathan R, Selvakumar R, Manivannan K, Nithyanantham R, Kaverinathan K. Behaviour of soil borne inoculum of *Colletotrichum falcatum* in causing red rot in sugarcane varieties with varying disease resistance. Sugar Tech. 2020;22(3):485-97. https://doi.org/10.1007/s12355-020-00800-7
9. Shukla S, Upadhyay D, Mishra A, Jindal T, Shukla K. Challenges faced by farmers in crops production due to fungal pathogens and their effect on Indian economy. InFungal diversity, ecology and control management 2022:495-505. Singapore: Springer Nature Singapore. https://doi.org/10.1007/978-981-16-8877-5_24
10. Kamle M, Kumar P. *Colletotrichum gloeosporioides*: pathogen of anthracnose disease in mango (*Mangifera indica* L.). InCurrent trends in plant disease diagnostics and management practices 2016: 207-219. Cham: Springer International Publishing. https://doi.org/10.1007/978-3-319-27312-9_9
11. Zrenner R, Genzel F, Verwaaijen B, Wibberg D, Grosch R. Necrotrophic lifestyle of *Rhizoctonia solani* AG3-PT during interaction with its host plant potato as revealed by transcriptome analysis. Scientific reports. 2020;10(1):12574. https://doi.org/10.1038/s41598-020-68728-2
12. Trkulja V, Cojic B, Trkulja N, Tomic A, Matic S, Ikanovic J, Popovic Milovanovic T. *Colletotrichum* species associated with apple bitter rot and *Glomerella* leaf spot: A comprehensive overview. Journal of Fungi. 2024;10(9):660. https://doi.org/10.3390/jof10090660
13. Abdelaziz AM, El-Wakil DA, Hashem AH, Al-Askar AA, AbdElgawad H, Attia MS. Efficient role of endophytic *Aspergillus terreus* in biocontrol of Rhizoctonia solani causing damping-off disease of *Phaseolus vulgaris* and *Vicia faba*. Microorganisms. 2023;11(6):1487. https://doi.org/10.3390/microorganisms11061487.
14. El-Baky NA, Amara AA. Recent approaches towards control of fungal diseases in plants: An updated review. Journal of Fungi. 2021;7(11):900. https://doi.org/10.3390/jof7110900
15. Naziya B, Murali M, Amruthesh KN. Plant growth-promoting fungi (PGPF) instigate plant growth and induce disease resistance in *Capsicum annuum* L. upon infection with *Colletotrichum capsici* (Syd.) Butler & Bisby. Biomolecules. 2019;10(1):41. https://doi.org/10.3390/biom10010041

16. Li Z, Bi X, Dai Y, Ren R. Enhancing mango anthracnose control and quality maintenance through chitosan and iturin A coating. Lwt. 2024;198:115955. https://doi.org/10.1016/j.lwt.2024.115955
17. Sanchez-Torres P. Emerging alternatives to control fungal contamination. Current Opinion in Food Science. 2025;61:101255. https://doi.org/10.1016/j.cofs.2024.101255
18. Hofmann T, Lowry GV, Ghoshal S, Tufenkji N, Brambilla D, Dutcher JR, Gilbertson LM, Giraldo JP, Kinsella JM, Landry MP, Lovell W. Technology readiness and overcoming barriers to sustainably implement nanotechnology-enabled plant agriculture. Nature Food. 2020;1(7):416-25. https://doi.org/10.1038/s43016-020-0110-1
19. Pereira AD, Oliveira HC, Fraceto LF. Polymeric nanoparticles as an alternative for application of gibberellic acid in sustainable agriculture: a field study. Scientific reports. 2019;9(1):7135. https://doi.org/10.1038/s41598-019-43494-y
20. Kumar S, Nehra M, Dilbaghi N, Marrazza G, Hassan AA, Kim KH. Nano-based smart pesticide formulations: Emerging opportunities for agriculture. Journal of controlled release. 2019;294:131-53. https://doi.org/10.1016/j.jconrel.2018.12.012
21. Izuafa A, Chimbekujwo KI, Raji RO, Oyewole OA, Oyewale RO, Abioye OP. Application of nanoparticles for targeted management of pests, pathogens and disease of plants. Plant Nano Biology. 2025:100177. https://doi.org/10.1016/j.plana.2025.100177
22. Al-Amri N, Tombuloglu H, Slimani Y, Akhtar S, Barghouthi M, Almessiere M, Alshammari T, Baykal A, Sabit H, Ercan I, Ozcelik S. Size effect of iron (III) oxide nanomaterials on the growth, and their uptake and translocation in common wheat (*Triticum aestivum* L.). Ecotoxicology and environmental safety. 2020;194:110377. https://doi.org/10.1016/j.ecoenv.2020.110377
23. Davila Costa JS, Romero CM. Nano-biofungicides and bio-nanofungicides: state of the art of innovative tools for controlling resistant phytopathogens. Biophysica. 2025;5(2):15. https://doi.org/10.3390/biophysica5020015
24. Joudeh N, Linke D. Nanoparticle classification, physicochemical properties, characterization, and applications: a comprehensive review for biologists. Journal of nanobiotechnology. 2022;20(1):262. https://doi.org/10.1186/s12951-022-01477-8
25. Asif N, Amir M, Fatma T. Recent advances in the synthesis, characterization and biomedical applications of zinc oxide nanoparticles. Bioprocess and Biosystems Engineering. 2023;46(10):1377-98. https://doi.org/10.1007/s00449-023-02886-1
26. Murali M, Kalegowda N, Gowtham HG, Ansari MA, Alomary MN, Alghamdi S, Shilpa N, Singh SB, Thriveni MC, Aiyaz M, Angaswamy N. Plant-mediated zinc oxide nanoparticles: advances in the new millennium towards understanding their therapeutic role in biomedical applications. Pharmaceutics. 2021;13(10):1662. https://doi.org/10.3390/pharmaceutics13101662
27. Mohammed AM, Mohammed M, Oleiwi JK, Ihmedee FH, Adam T, Betar BO, Gopinath SC. Comprehensive review on zinc oxide nanoparticle production and the associated antibacterial mechanisms and therapeutic potential. Nano Trends. 2025:100145. https://doi.org/10.1016/j.nwnano.2025.100145
28. Sharma R, Kumar N, Sharma P, Yadav A, Aggarwal NK. Biosynthesis, characterisation and therapeutic potential of green coconut waste derived zinc oxide nanoparticles. Results in Surfaces and Interfaces. 2025;18:100372. https://doi.org/10.1016/j.rsurfi.2024.100372
29. Ragavendran C, Kamaraj C, Jothimani K, Priyadharsan A, Kumar DA, Natarajan D, Malafaia G. Eco-friendly approach for ZnO nanoparticles synthesis and evaluation of its possible antimicrobial, larvicidal and photocatalytic applications. Sustainable Materials and Technologies. 2023;36:e00597. https://doi.org/10.1016/j.susmat.2023.e00597
30. Naseer M, Aslam U, Khalid B, Chen B. Green route to synthesize Zinc Oxide Nanoparticles using leaf extracts of *Cassia fistula* and *Melia azadarach* and their antibacterial potential. Scientific Reports. 2020;10(1):9055. https://doi.org/10.1038/s41598-020-65949-3

31. Udayagiri H, Sana SS, Dogiparthi LK, Vadde R, Varma RS, Koduru JR, Ghodake GS, Somala AR, Boya VK, Kim SC, Karri RR. Phytochemical fabrication of ZnO nanoparticles and their antibacterial and anti-biofilm activity. Scientific Reports. 2024;14(1):19714. https://doi.org/10.1038/s41598-024-69044-9
32. Roy P, Das B, Mohanty A, Mohapatra S. Green synthesis of silver nanoparticles using *Azadirachta indica* leaf extract and its antimicrobial study. Applied Nanoscience. 2017;7(8):843-50. https://doi.org/10.1007/s13204-017-0621-8
33. Iqbal Y, Malik AR, Iqbal T, Aziz MH, Ahmed F, Abolaban FA, Ali SM, Ullah H. Green synthesis of ZnO and Ag-doped ZnO nanoparticles using *Azadirachta indica* leaves: Characterization and their potential antibacterial, antidiabetic, and wound-healing activities. Materials Letters. 2021;305:130671. https://doi.org/10.1016/j.matlet.2021.130671
34. El-Beltagi HS, Ragab M, Osman A, El-Masry RA, Alwutayd KM, Althagafi H, Alqahtani LS, Alazragi RS, Alhajri AS, El-Saber MM. Biosynthesis of zinc oxide nanoparticles via neem extract and their anticancer and antibacterial activities. PeerJ. 2024;12:e17588. https://doi.org/10.7717/peerj.17588
35. Elumalai K, Velmurugan S. Green synthesis, characterization and antimicrobial activities of zinc oxide nanoparticles from the leaf extract of *Azadirachta indica* (L.). Applied Surface Science. 2015;345:329-36. https://doi.org/10.1016/j.apsusc.2015.03.176
36. Sanjeev NO, Valsan AE, Zachariah S, Vasu ST. Synthesis of zinc oxide nanoparticles from *Azadirachta indica* extract: a sustainable and cost-effective material for wastewater treatment. Journal of Hazardous, Toxic, and Radioactive Waste. 2023;27(4):04023027. https://doi.org/10.1061/JHTRBP.HZENG-1217
37. Tsegahun E, Aklilu M. Neem (*Azadirachta indica*) leaf extract mediated synthesis of zinc oxide nanoparticles (ZnO NPs) and their antibacterial activity. Discover Nano. 2025;20(1):145. https://doi.org/10.1186/s11671-025-04260-4
38. Bhuyan T, Mishra K, Khanuja M, Prasad R, Varma A. Biosynthesis of zinc oxide nanoparticles from *Azadirachta indica* for antibacterial and photocatalytic applications. Materials Science in Semiconductor Processing. 2015;32:55-61. https://doi.org/10.1016/j.mssp.2014.12.053
39. Ali J, Mazumder JA, Perwez M, Sardar M. Antimicrobial effect of ZnO nanoparticles synthesized by different methods against food borne pathogens and phytopathogens. Materials Today: Proceedings. 2021;36:609-15. https://doi.org/10.1016/j.matpr.2020.03.173
40. Mariyam S, Upadhyay SK, Chakraborty K, Verma KK, Duhan JS, Muneer S, Meena M, Sharma RK, Ghodake G, Seth CS. Nanotechnology, a frontier in agricultural science, a novel approach in abiotic stress management and convergence with new age medicine-A review. Science of the Total Environment. 2024;912:169097. https://doi.org/10.1016/j.scitotenv.2023.169097
41. Yadav M. Nanoparticle-facilitated targeted nutrient delivery in plants: Breakthroughs and mechanistic insights. Plant Nano Biology. 2025;12:100156. https://doi.org/10.1016/j.plana.2025.100156
42. Atanda SA, Shaibu RO, Agunbiade FO. Nanoparticles in agriculture: balancing food security and environmental sustainability. Discover Agriculture. 2025;3(1):26. https://doi.org/10.1007/s44279-025-00159-x
43. Rai-Kalal P, Jajoo A. Priming with zinc oxide nanoparticles improve germination and photosynthetic performance in wheat. Plant Physiology and Biochemistry. 2021;160:341-51. https://doi.org/10.1016/j.plaphy.2021.01.032
44. Nile SH, Thiruvengadam M, Wang Y, Samynathan R, Shariati MA, Rebezov M, Nile A, Sun M, Venkidasamy B, Xiao J, Kai G. Nano-priming as emerging seed priming technology for sustainable agriculture—recent developments and future perspectives. Journal of nanobiotechnology. 2022;20(1):254. https://doi.org/10.1186/s12951-022-01423-8

45. Awan S, Shahzadi K, Javad S, Tariq A, Ahmad A, Ilyas S. A preliminary study of influence of zinc oxide nanoparticles on growth parameters of *Brassica oleracea* var italic. Journal of the Saudi Society of Agricultural Sciences. 2021;20(1):18-24. https://doi.org/10.1016/j.jssas.2020.10.003
46. Geremew A, Carson L, Woldesenbet S, Wang H, Reeves S, Brooks Jr N, Saganti P, Weerasooriya A, Peace E. Effect of zinc oxide nanoparticles synthesized from *Carya illinoinensis* leaf extract on growth and antioxidant properties of mustard (*Brassica juncea*). Frontiers in Plant Science. 2023;14:1108186. https://doi.org/10.3389/fpls.2023.1108186
47. Regni L, Del Buono D, Micheli M, Facchin SL, Tolisano C, Proietti P. Effects of biogenic ZnO nanoparticles on growth, physiological, biochemical traits and antioxidants on olive tree in vitro. Horticulturae. 2022;8(2):161. https://doi.org/10.3390/horticulturae8020161
48. Hamzah Saleem M, Usman K, Rizwan M, Al Jabri H, Alsafran M. Functions and strategies for enhancing zinc availability in plants for sustainable agriculture. Frontiers in Plant Science. 2022;13:1033092. https://doi.org/10.3389/fpls.2022.1033092
49. Al-Harbi HF, Awad MA, Ortashi KM, Al-Humaid LA, Ibrahim AA, Al-Huqail AA. Green synthesis of zinc oxide nanoparticles: physicochemical Characterization, photocatalytic Performance, and evaluation of their impact on seed germination parameters in crops. Catalysts. 2025;15(10):924. https://doi.org/10.3390/catal15100924
50. Mahra S, Tripathi S, Tiwari K, Sharma S, Mathew S, Kumar V, Sharma S. Harnessing nanotechnology for sustainable agriculture: from seed priming to encapsulation. Plant Nano Biology. 2025;11:100124. https://doi.org/10.1016/j.plana.2024.100124
51. Kim SH, Bae S, Sung YW, Hwang YS. Effects of particle size on toxicity, bioaccumulation, and translocation of zinc oxide nanoparticles to bok choy (*Brassica chinensis* L.) in garden soil. Ecotoxicology and Environmental Safety. 2024;280:116519. https://doi.org/10.1016/j.ecoenv.2024.116519
52. Khalid F, Asif K, Rasheed Y, Ashraf H, Maqsood MF, Rana S, Zulfiqar U, Naz N, Shahbaz M, Sardar R, Riaz Z. Nano priming for boosting growth and resilience in crops under abiotic stresses. Biocatalysis and Agricultural Biotechnology. 2023;53:102892. https://doi.org/10.1016/j.bcab.2023.102892
53. Pandya P, Kumar S, Patil G, Mankad M, Shah Z. Impact of ZnO nanopriming on physiological and biochemical traits of wheat (*Triticum aestivum* L.) seedling. CABI Agriculture and Bioscience. 2024;5(1):27. https://doi.org/10.1186/s43170-024-00228-z
54. Joesna G, Alodhayb A, Sasikumar P, Sree TL, Ferin RZ, Sankar D, Prabakaran A, Prasath M, Muthuramamoorthy M, Mohamed MG, Vimalan M. Bio-synthesis zinc oxide nanoparticle: *Azadirachta indica* and *Phyllanthus acidus* mediated green approach for enhanced biological efficacy. Chemical Physics Impact. 2025;10:100821. https://doi.org/10.1016/j.chphi.2025.100821
55. Abdelbaky AS, Abd El-Mageed TA, Babalghith AO, Selim S, Mohamed AM. Green synthesis and characterization of ZnO nanoparticles using *Pelargonium odoratissimum* (L.) aqueous leaf extract and their antioxidant, antibacterial and anti-inflammatory activities. Antioxidants. 2022;11(8):1444. https://doi.org/10.3390/antiox11081444
56. Vikal S, Gautam YK, Kumar A, Kumar A, Singh J, Pratap D, Singh BP, Singh N. Bioinspired palladium-doped manganese oxide nanocorns: a remarkable antimicrobial agent targeting phyto/animal pathogens. Scientific Reports. 2023;13(1):14039. https://doi.org/10.1038/s41598-023-40822-1
57. Ouf MS, Duab ME, Abdel-Meguid DI, El-Sharouny EE, Soliman NA. Biogenic Zinc nanoparticles: green approach to synthesis, characterization, and antimicrobial applications. Microbial Cell Factories. 2025;24(1):168. https://doi.org/10.1186/s12934-025-02788-9
58. Singh J, Kumar A, Nayal AS, Vikal S, Shukla G, Singh A, Singh A, Goswami S, Kumar A, Gautam YK, Verma Y. Comprehensive antifungal investigation of green synthesized silver nanoformulation

against four agriculturally significant fungi and its cytotoxic applications. Scientific Reports. 2024;14(1):5934. https://doi.org/10.1038/s41598-024-56619-9
59. Elshafie HS, Osman A, El-Saber MM, Camele I, Abbas E. Antifungal activity of green and chemically synthesized ZnO nanoparticles against *Alternaria citri*, the causal agent citrus black rot. The Plant Pathology Journal. 2023;39(3):265. https://doi.org/10.5423/PPJ.OA.02.2023.0035.
60. Chowdappa P, Gowda S, Chethana CS, Madhura S. Antifungal activity of chitosan-silver nanoparticle composite against *Colletotrichum gloeosporioides* associated with mango anthracnose. African Journal of Microbiology Research. 2014;8(17):1803-12. https://doi.org/10.5897/AJMR2013.6584
61. Kora AJ, Mounika J, Jagadeeshwar R. Rice leaf extract synthesized silver nanoparticles: An in vitro fungicidal evaluation against *Rhizoctonia solani*, the causative agent of sheath blight disease in rice. Fungal biology. 2020;124(7):671-81. https://doi.org/10.1016/j.funbio.2020.03.012
62. Jayaprakashvel M, Sharmika N, Vinothini S, Venkatramani M, Muthezhilan R, Hussain AJ. Biological control of sheath blight of rice using marine associated *Fluorescent pseudomonads*. Biosci Biotechnol Res Asia. 2014;11:115-21. https://doi.org/10.13005/bbra/1399
63. IRRI I. Standard evaluation system for rice. International Rice Research Institute, Philippine. 2002:1-45. https://www.knowledgebank.irri.org/images/docs/rice-standard-evaluation-system.pdf
64. Wlodarczyk K, Smolinska B. The effect of nano-ZnO on seeds germination parameters of different tomatoes (*Solanum lycopersicum* L.) cultivars. Molecules. 2022;27(15):4963. https://doi.org/10.3390/molecules27154963
65. Jayachandran A, Aswathy TR, Nair AS. Green synthesis and characterization of zinc oxide nanoparticles using *Cayratia pedata* leaf extract. Biochemistry and Biophysics Reports. 2021;26:100995. https://doi.org/10.1016/j.bbrep.2021.100995
66. Abdelmigid HM, Hussien NA, Alyamani AA, Morsi MM, AlSufyani NM, Kadi HA. Green synthesis of zinc oxide nanoparticles using pomegranate fruit peel and solid coffee grounds vs. chemical method of synthesis, with their biocompatibility and antibacterial properties investigation. Molecules. 2022;27(4):1236. https://doi.org/10.3390/molecules27041236
67. Karam ST, Abdulrahman AF. Green synthesis and characterization of ZnO nanoparticles by using thyme plant leaf extract. InPhotonics 2022;9(8):594. https://doi.org/10.3390/photonics9080594
68. Chikkanna MM, Neelagund SE, Rajashekarappa KK. Green synthesis of zinc oxide nanoparticles (ZnO NPs) and their biological activity. SN Applied Sciences. 2019;1(1):117. https://doi.org/10.1007/s42452-018-0095-7
69. Singh A, Kaushik M. Physicochemical investigations of zinc oxide nanoparticles synthesized from *Azadirachta indica* (Neem) leaf extract and their interaction with Calf-Thymus DNA. Results in Physics. 2019;13:102168. https://doi.org/10.1016/j.rinp.2019.102168
70. Yadeta Gemachu L, Lealem Birhanu A. Green synthesis of ZnO, CuO and NiO nanoparticles using Neem leaf extract and comparing their photocatalytic activity under solar irradiation. Green Chemistry Letters and Reviews. 2024;17(1):2293841. https://doi.org/10.1080/17518253.2023.2293841
71. Fugare AG, Shete RV, Adak VS, Murthy G K. A review on *Pongamia pinnata* (L.): Traditional uses, phytochemistry and pharmacological properties. Journal of Drug Delivery & Therapeutics. 2021;11(1-s):207-211. https://doi.org/10.22270/jddt.v11i1-s.4522
72. Taniguchi M, LaRocca CA, Bernat JD, Lindsey JS. Digital database of absorption spectra of diverse flavonoids enables structural comparisons and quantitative evaluations. Journal of Natural Products. 2023;86(4):1087-119. https://doi.org/10.1021/acs.jnatprod.2c00720

73. Dodoo-Arhin D, Asiedu T, Agyei-Tuffour B, Nyankson E, Obada D, Mwabora JM. Photocatalytic degradation of Rhodamine dyes using zinc oxide nanoparticles. Materials Today: Proceedings. 2021;38:809-15. https://doi.org/10.1016/j.matpr.2020.04.597
74. Tran XT, Bien TT, Van Tran T, Nguyen TT. Biosynthesis of ZnO nanoparticles using aqueous extracts of *Eclipta prostrata* and *Piper longum*: characterization and assessment of their antioxidant, antibacterial, and photocatalytic properties. Nanoscale Advances. 2024;6(19):4885-99. https://doi.org/10.1039/D4NA00326H
75. Sengupta A, Sarkar A. Synthesis and characterization of nanoparticles from neem leaves and banana peels: a green prospect for dye degradation in wastewater. Ecotoxicology. 2022;31(4):537-48. https://doi.org/10.1007/s10646-021-02414-5
76. El-Belely EF, Farag MM, Said HA, Amin AS, Azab E, Gobouri AA, Fouda A. Green synthesis of zinc oxide nanoparticles (ZnO-NPs) using *Arthrospira platensis* (Class: Cyanophyceae) and evaluation of their biomedical activities. Nanomaterials. 2021;11(1):95. https://doi.org/10.3390/nano11010095
77. Barzinjy AA, Azeez HH. Green synthesis and characterization of zinc oxide nanoparticles using *Eucalyptus globulus* Labill. leaf extract and zinc nitrate hexahydrate salt. SN Applied Sciences. 2020;2(5):991. https://doi.org/10.1007/s42452-020-2813-1
78. Ahmad N, Ali S, Abbas M, Fazal H, Saqib S, Ali A, Ullah Z, Zaman S, Sawati L, Zada A, Sohail. Antimicrobial efficacy of *Mentha piperata*-derived biogenic zinc oxide nanoparticles against UTI-resistant pathogens. Scientific Reports. 2023;13(1):14972. https://doi.org/10.1038/s41598-023-41502-w
79. Akber MA, Mubeen M, Sohail MA, Khan SW, Solanki MK, Khalid R, Abbas A, Divvela PK, Zhou L. Global distribution, traditional and modern detection, diagnostic, and management approaches of *Rhizoctonia solani* associated with legume crops. Frontiers in Microbiology. 2023;13:1091288. https://doi.org/10.3389/fmicb.2022.1091288
80. Hossain MM, Sultana F, Li W, Tran LS, Mostofa MG. *Sclerotinia sclerotiorum* (Lib.) de Bary: Insights into the pathogenomic features of a global pathogen. Cells. 2023;12(7):1063. https://doi.org/10.3390/cells12071063
81. Law CX, Hashim N, Ismail SI, Jahari M, Al Riza DF. A review on anthracnose disease caused by *Colletotrichum* spp. in fruits and advances in control strategies. International Journal of Food Microbiology. 2025:111397. https://doi.org/10.1016/j.ijfoodmicro.2025.111397
82. Naiel B, Fawzy M, Halmy MW, Mahmoud AE. Green synthesis of zinc oxide nanoparticles using Sea Lavender (*Limonium pruinosum* L. Chaz.) extract: characterization, evaluation of anti-skin cancer, antimicrobial and antioxidant potentials. Scientific Reports. 2022;12(1):20370. https://doi.org/10.1038/s41598-022-24805-2
83. Bouttier-Figueroa DC, Cortez-Valadez M, Flores-Acosta M, Robles-Zepeda RE. Green synthesis of zinc oxide nanoparticles using plant extracts and their antimicrobial activity. BioNanoScience. 2024;14(3):3385-400. https://doi.org/10.1007/s12668-024-01471-4
84. Macan GP, Khalil S, Kalyandurg PB, Pareek N, Vetukuri RR. A detached leaf assay for rapidly screening plant pathogen-biological control agents. InPlant Pathology: Method and Protocols 2022;2536:449-458. New York, NY: Springer US. https://doi.org/10.1007/978-1-0716-2517-0_26.
85. Divya S, Anusree AR, Vigi S, Jiji SG, Das PA, Dev AR, Thara SS, Varghese EM, Gopinath PP, Anith KN. Silver nanoparticles green synthesized with leaf extract of disease-resistant amaranthus genotypes effectively suppress leaf blight (*Rhizoctonia solani* Kuhn) disease in a susceptible red amaranthus cultivar. 3 Biotech. 2023;13(6):196. https://doi.org/10.1007/s13205-023-03614-y
86. Chandra S, Chakraborty N, Dasgupta A, Sarkar J, Panda K, Acharya K. Chitosan nanoparticles: a positive modulator of innate immune responses in plants. Scientific reports. 2015;5(1):15195. https://doi.org/10.1038/srep15195

87. Sathiyabama M, Boomija RV, Muthukumar S, Gandhi M, Salma S, Prinsha TK, Rengasamy B. Green synthesis of chitosan nanoparticles using tea extract and its antimicrobial activity against economically important phytopathogens of rice. Scientific Reports. 2024;14(1):7381. https://doi.org/10.1038/s41598-024-58066-y
88. Chiranjeevi N, Kumar PA, Jayalakshmi RS, Prasad KH, Prasad TN. Bio efficacy of biogenic silver nanoparticles against rice sheath blight causing pathogen *Rhizoctonia solani* Kuhn. International Journal of Current Microbiology and Applied Sciences. 2018;7(7):4148-60. https://doi.org/10.20546/ijcmas.2018.707.484
89. Divya K, Thampi M, Vijayan S, Varghese S, Jisha MS. Induction of defence response in *Oryza sativa* L. against *Rhizoctonia solani* (Kuhn) by chitosan nanoparticles. Microbial Pathogenesis. 2020;149:104525. https://doi.org/10.1016/j.micpath.2020.104525
90. Sahgal M, Saini N, Jaggi V, Brindhaa NT, Kabdwal M, Singh RP, Prakash A. Antagonistic potential and biological control mechanisms of *Pseudomonas* strains against banded leaf and sheath blight disease of maize. Scientific Reports. 2024;14(1):13580. https://doi.org/10.1038/s41598-024-64028-1
91. Su Y, Ashworth V, Kim C, Adeleye AS, Rolshausen P, Roper C, White J, Jassby D. Delivery, uptake, fate, and transport of engineered nanoparticles in plants: a critical review and data analysis. Environmental Science: Nano. 2019;6(8):2311-31. https://doi.org/10.1039/C9EN00461K
92. Puangpathumanond S, Chee HL, Sevencan C, Yang X, Lau OS, Lew TT. Stomata-targeted nanocarriers enhance plant defense against pathogen colonization. Nature Communications. 2025;16(1):4816. https://doi.org/10.1038/s41467-025-60112-w
93. Lv X, Sha H, Ye Z, Wang Y, Mao B. Nanomaterials in plant management: functions, mechanisms and prospects. Environmental Science: Nano. 2023;10(12):3232-52. https://doi.org/10.1039/D3EN00014A
94. Mahakham W, Sarmah AK, Maensiri S, Theerakulpisut P. Nanopriming technology for enhancing germination and starch metabolism of aged rice seeds using phytosynthesized silver nanoparticles. Scientific reports. 2017;7(1):8263. https://doi.org/10.1038/s41598-017-08669-5
95. El-Badri AM, Batool M, Wang C, Hashem AM, Tabl KM, Nishawy E, Kuai J, Zhou G, Wang B. Selenium and zinc oxide nanoparticles modulate the molecular and morpho-physiological processes during seed germination of *Brassica napus* under salt stress. Ecotoxicology and Environmental Safety. 2021;225:112695. https://doi.org/10.1016/j.ecoenv.2021.112695
96. Muhammad M, Waheed A, Wahab A, Majeed M, Nazim M, Liu YH, Li L, Li WJ. Soil salinity and drought tolerance: An evaluation of plant growth, productivity, microbial diversity, and amelioration strategies. Plant Stress. 2024;11:100319. https://doi.org/10.1016/j.stress.2023.100319

Supplementary Files

This is a list of supplementary files associated with this preprint. Click to download.

- Supplementary.docx